AGU PUBLICATIONS

JGR

Journal of Geophysical Research: Space Physics

RESEARCH ARTICLE
10.1002/2013JA019393

Special Section:
Fundamental Properties and Processes of Magnetotails

Key Points:
- We have studied the properties of plasmoids observed in Jupiter's magnetotail
- The average mass lost and flux closed is compared to estimated inputs
- Jovian plasmoids play a major role in flux transport but not in mass transport

Correspondence to:
M. F. Vogt,
marissa.vogt@ion.le.ac.uk

Citation:
Vogt, M. F., C. M. Jackman, J. A. Slavin, E. J. Bunce, S. W. H. Cowley, M. G. Kivelson, and K. K. Khurana (2014), Structure and statistical properties of plasmoids in Jupiter's magnetotail, *J. Geophys. Res. Space Physics*, *119*, 821–843, doi:10.1002/2013JA019393.

Received 31 AUG 2013
Accepted 10 JAN 2014
Accepted article online 13 JAN 2014
Published online 5 FEB 2014

Structure and statistical properties of plasmoids in Jupiter's magnetotail

Marissa F. Vogt[1], Caitriona M. Jackman[2,3,4], James A. Slavin[5], Emma J. Bunce[1], Stanley W. H. Cowley[1], Margaret G. Kivelson[5,6,7], and Krishan K. Khurana[5,6]

[1]Department of Physics and Astronomy, University of Leicester, Leicester, UK, [2]Department of Physics and Astronomy, University College London, London, UK, [3]Centre for Planetary Sciences, UCL/Birkbeck, London, UK, [4]Now at University of Southampton, Southampton, UK, [5]Department of Atmospheric, Oceanic, and Space Science, University of Michigan, Ann Arbor, Michigan, USA, [6]Department of Earth, Planetary, and Space Sciences, University of California, Los Angeles, California, USA, [7]Institute of Geophysics and Planetary Physics, University of California, Los Angeles, California, USA

Abstract Plasmoids and other reconnection-related signatures have been observed in Jupiter's magnetotail through analysis of magnetic field and energetic particle data. Previous studies have established the spatial distribution and recurrence period of tail reconnection events, and identified the location of a statistical X-line separating inward and outward flow. Here we present new analysis focusing specifically on 43 plasmoid signatures observed in magnetometer data in order to establish the average properties and internal structure of Jovian plasmoids. We present statistics on the observed plasmoid length scale, duration, radial position, and local time distribution. On average, the observed plasmoids have a ~3 R_J radial extent and ~7 min duration and result in the closure of ~4–8 GWb of open flux from reconnection of open field lines in the postplasmoid plasma sheet. We also determine the amount of mass released and the magnetic flux closed in order to understand the role of tail reconnection in the transport of mass and flux in Jupiter's magnetosphere. The observed plasmoid properties are consistent with a mass loss rate of ~0.7–120 kg/s and a flux closure rate of ~7–70 GWb/d. We conclude that tail reconnection and plasmoid release is an important method of flux transport at Jupiter but likely cannot account for the mass input from Io, suggesting that additional mass loss mechanisms may be significant. Finally, we examine the plasmoid interior structure through minimum variance analysis and find that most plasmoids lack a core field and are better described by magnetic loops rather than flux ropes.

1. Introduction

Magnetic reconnection in planetary magnetotails is an important physical process that allows for the release of mass and energy from the system. Reconnection signatures have been observed in magnetic field and particle measurements at the Earth [e.g., *Angelopoulos et al*., 2008; review by *Sharma et al*., 2008 and references therein], Mercury [*Slavin et al*., 2009, 2012], Jupiter [*Russell et al*., 1998], and Saturn [*Jackman et al*., 2007], though at each planet the factors which drive tail reconnection are thought to be quite different. One common feature has been the identification of plasmoids [*Hones*, 1976; 1977], structures which form when part of the plasma sheet breaks off, releasing a plasma bubble on closed loops of disconnected field lines that can be ejected down the tail.

Analysis of in situ magnetic field and particle data at Jupiter has established the spatial distribution and typical recurrence period of the observed reconnection signatures, and identified the location of a statistical X line separating inward and outward flow [*Woch et al*., 2002; *Kronberg et al*., 2005, 2007, 2008a; *Vogt et al*., 2010]. A subset of the observed reconnection events has been classified as plasmoids, which are identified in magnetic field data by a characteristic bipolar signature in the north–south component of the magnetic field. However, the structure of Jovian plasmoids and their role in the overall mass and flux transport at Jupiter have not been examined in great detail. Therefore, in this study we analyze the plasmoids detected in Jupiter's magnetotail and present statistics on the observed length scale, duration, spatial distribution, and the amount of mass released and magnetic flux closed due to reconnection of open field lines following a typical plasmoid event. The results can then be compared to the mass loading rate from Io, ~500–1000 kg/s [e.g., *Thomas et al*., 2004], and estimates of the rate of flux opened by reconnection with the solar wind [e.g., *Nichols et al*., 2006; *Badman and Cowley*, 2007] to determine the importance of the observed plasmoids to the

overall mass and flux transport at Jupiter. Through both a superposed epoch analysis of 43 plasmoids and individual case studies, we examine the typical interior structure of the plasmoids, determine whether they are best described as magnetic flux ropes or loops, and discuss the implications for the large-scale magnetotail structure.

We begin in section 2 with a review of the present models of Jovian tail dynamics and studies of reconnection signatures from in situ particle and magnetometer data. In section 3 we explain how we selected the plasmoids studied here, illustrate the expected magnetic field signature of a plasmoid and how it can be affected by the spacecraft trajectory, and present a case study example. The plasmoid statistical properties and interior structure, as well as a superposed epoch analysis of the 43 Jovian plasmoids, are presented in section 4. Finally, in section 5 we discuss the role of plasmoids in the mass and flux transport at Jupiter and comment on the local time distribution of the plasmoids and other reconnection signatures.

2. Background

2.1. Tail Reconnection at Jupiter: In Situ and Remote Observations

Surveys of in situ magnetic field and particle measurements in Jupiter's magnetosphere have found reconnection signatures across the nightside and at nearly all radial distances in the middle and outer magnetosphere for which there is data coverage [e.g., *Russell et al*., 1998; *Kronberg et al*., 2005, 2008a; *Ge et al*., 2007; *Vogt et al*., 2010]. These studies have also shown that Jovian tail reconnection is a fairly common process, with typical recurrence periods of a few days. Most of the reconnection events were identified in data from the Galileo spacecraft, which orbited Jupiter from late 1995 to 2003, though a few dynamic intervals were also observed during the Voyager 1 and 2 flybys in 1979 [*Nishida*, 1983].

In particle measurements, reconnection events have been identified by increases in radial particle flux anisotropies from which planetward or tailward flow can be inferred [*Woch et al*., 2002; *Kronberg et al*., 2005]. In magnetometer data the characteristic signature is an increase in $|B_\theta|$, the $\hat{\theta}$ component of the magnetic field in spherical polar coordinates referenced to Jupiter's spin axis, without a corresponding increase in the field magnitude, indicating reconfiguration to a more dipolar field [*Vogt et al*., 2010]. The azimuthal field component, B_φ, may also change as the field becomes more bent back or bent forward to conserve angular momentum as plasma is transported radially (see discussion in *Vogt et al*. [2010, section 3.4]).

The available magnetic field and particle measurements show generally good agreement, both for identifying intervals of tail dynamics and for inferring the radial flow direction and position relative to a reconnection X-line [*Kronberg et al*., 2008a; *Vogt et al*., 2010]. Most of the intervals of high radial anisotropy studied by *Kronberg et al*. [2005] were accompanied by field dipolarizations or reversals, and the flow direction inferred from the anisotropies was consistent with the changes seen in the magnetic field. Though the magnetometer does not directly measure flow, the radial flow direction can be inferred through the sign of B_θ, as illustrated in Figure 1. Jupiter's equatorial field is southward (oppositely oriented to the Earth's) so that the undisturbed background B_θ is positive, and planetward (tailward) of the X-line, it is most likely that B_θ will be positive (negative) and the radial flow will be inward (outward). However, it should be noted that a positive B_θ signature may be recorded at the tailward edge of the plasmoid, but in this case the positive B_θ signature would likely be followed by a field reversal and an interval of negative B_θ as the plasmoid moves radially outward. Such agreement is also found from studies of bursty bulk flows at the Earth, where the flow direction and sign of the north–south magnetic field component frequently agree [e.g., *Hones*, 1977; *Richardson et al*., 1987; *Angelopoulos et al*., 1994].

Woch et al. [2002], using flow burst measurements, and *Vogt et al*. [2010], using the inferred flow direction from magnetometer data, have identified the statistical location of the reconnection X-line. Near dawn, the X-line is located near 90 R_J (1 R_J = 71,492 km) and moves outward at earlier local times, close to ~100 R_J at midnight and ~120 R_J at 22:00 LT. From 18:00 to 22:00, there is insufficient data coverage to determine the location of the X-line. Most events in that local time sector were observed inside of ~90 R_J and with an enhanced positive B_θ signature, suggesting that the X-line is typically located beyond ~90 R_J, but the limited radial coverage precludes further constraint.

It should be noted that not all of the field dipolarizations or reversals seen in the magnetometer data are accompanied by increased particle radial anisotropies. For example, *Vogt et al*. [2010] reported 188 additional

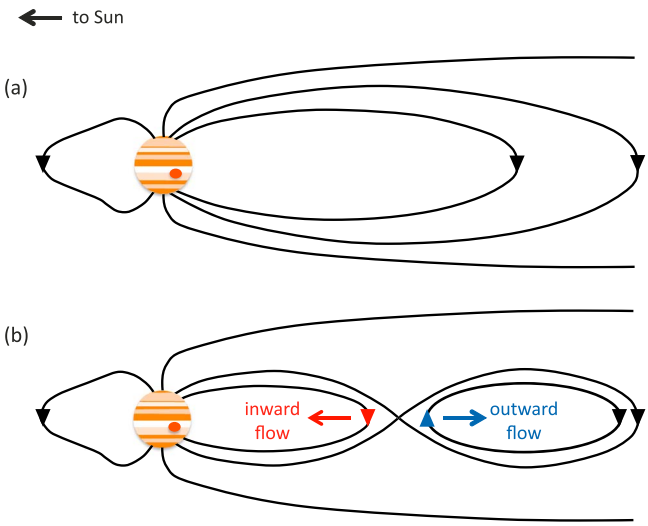

Figure 1. Schematic (not to scale) of reconnection in Jupiter's magnetotail, showing the noon-midnight meridian plane, with the Sun to the left. (a) The initial field configuration. (b) The field configuration and radial flow direction during reconnection. A positive B_θ, or southward field (red arrow), suggests that the spacecraft is planetward of the X-line and the plasma flow should be radially inward. Conversely, a negative B_θ, or northward field (blue arrow), suggests that the spacecraft is tailward of the X-line and the plasma flow should be radially outward. After *Vogt et al*. [2010, Figure 2].

reconnection events in the magnetometer data, as evidenced by increases in $|B_\theta|$ over background levels, which had not been previously identified in particle data. One possibility for the increased number of events identified by the magnetometer is that finer features can be resolved due to the higher time resolution of the magnetometer data (generally 24 s per vector) than for the particle data (3–11 min). Differences in the nature of reconnection signatures in the premidnight and postmidnight local time sectors may also explain the larger number of events found in the magnetometer data. *Kronberg et al*. [2005] reported only one premidnight reconfiguration event from particle anisotropies, while *Vogt et al*. [2010] identified 57 premidnight reconnection signatures in the magnetometer data. Recently, *Kasahara et al*. [2013] analyzed particle data from all of the *Vogt et al*. [2010] events, including the premidnight events not previously studied in the particle data, and reported that large density changes, indicating reconnection between the north and south lobes, and large radial flows were observed during the dawn sector events only. By comparison, for the dusk sector events the flow direction remained corotational, and little or no density change was observed. *Kasahara et al*. [2013] therefore proposed that another process—other than tail lobe reconnection—may be responsible for the duskside field dipolarization events.

In addition to the in situ evidence of tail reconnection, remote observations from the Hubble Space Telescope of Jupiter's ultraviolet aurora show polar spots that are thought to be associated with the inward flow from tail reconnection [*Grodent et al*., 2004; *Radioti et al*., 2008]. The emitted power of the spots is consistent with the field-aligned currents estimated from typical tail flow bursts [*Radioti et al*., 2010], and their ionospheric locations map to regions in the equatorial magnetosphere that are planetward of the statistical X-line [*Vogt et al*., 2011]. In one recent study of nightside UV and IR spots, *Radioti et al*. [2011] reported the presence of an auroral spot at nearly the same time that the Galileo magnetometer recorded a field dipolarization in the premidnight magnetotail and showed that the spot location magnetically mapped close to Galileo's position and inside of the statistical X-line.

In the absence of simultaneous multipoint measurements across Jupiter's magnetotail, it is extremely difficult to determine whether reconnection at Jupiter is a localized or global process. Rough estimates of the azimuthal extent, or flow channel width, based on the duration of observed individual reconnection events and the typical azimuthal flow speed, suggest that reconnection occurs over an area with a relatively narrow ~15–20 R_J region, or less than 10% of the magnetotail width [*Vogt et al*., 2010]. These estimates suggest that tail reconnection at Jupiter is a localized process and may be more comparable to reconnection-driven bursty bulk flows at Earth rather than terrestrial substorms, which involve reconnection across much of the magnetotail. Bursty bulk flows occur locally, typically spanning ~5–10% of the tail width [*Angelopoulos et al*., 1996], though multipoint

spacecraft measurements have recorded simultaneous flow bursts occurring across much of the tail [*Slavin et al*., 1997]. Auroral observations provide a way to remotely sense the state of Jupiter's entire magnetosphere and can therefore provide information about the flow channel azimuthal extent. For example, the polar auroral spots are relatively localized but have been observed simultaneously near dawn and premidnight, possibly indicating that reconnection can occur simultaneously in several narrow channels across Jupiter's magnetotail [*Radioti et al*., 2011].

2.2. Rotationally Versus Internally Driven Dynamics

It is generally agreed that centrifugal stresses play a significant role in driving dynamics in Jupiter's rapidly rotating magnetosphere (rotation period ~10 h), though there is considerable disagreement over the relative role of the solar wind in driving tail reconnection [e.g., *McComas and Bagenal*, 2007; *Cowley et al*., 2008]. In the model of internally driven reconnection typically called the Vasyliūnas cycle, tail reconnection occurs on closed field lines when mass-loaded flux tubes are stretched to the point where the centrifugal acceleration of particles on rotating flux tubes causes the tailward flow energy to exceed the energy in the closed magnetic field [*Vasyliūnas*, 1983]. The stretched flux tubes pinch off, or reconnect, releasing a plasmoid.

On long timescales, the flux opened by reconnection at the magnetopause must balance the flux closed via tail reconnection (or closed via magnetopause reconnection at high latitudes, e.g., *McComas and Bagenal* [2007]), to maintain the tail lobes and auroral polar cap. It is difficult to determine if there is any relationship on shorter timescales between the observed tail reconnection signatures and magnetic flux opening on the dayside in the absence of upstream solar wind measurements at Jupiter. However, the distribution of events in local time can provide clues to the possibility of solar wind driving via the Dungey cycle, in which magnetic flux is opened by reconnection with the solar wind on the dayside and closed due to reconnection at an X-line in the tail. *Cowley et al*. [2003] propose that at Jupiter, the Dungey cycle X-line would be restricted to the dawn local time sector. Dungey cycle reconnection between the tail lobes and the subsequent sunward transport of newly closed magnetic flux would therefore not be expected in the dusk and midnight sector because the strong outward flows associated with both corotation and the Vasyliūnas cycle would oppose sunward return flow from a reconnection X-line. Therefore, according to *Cowley et al*. [2003], reconnection signatures observed at premidnight local times are more likely to be associated with internal driving.

The periodic recurrence of reconnection events can also be used to infer the relative importance of internal versus solar wind driving. *Kronberg et al*. [2007] calculated a characteristic timescale of a few days for an internally driven mass loading and release process model, and this timescale is similar to observed periodicities observed from several data sets. A 2–3 day periodicity has been seen in flow bursts inferred through particle anisotropies [*Krupp et al*., 1998; *Woch et al*., 1998; *Kronberg et al*., 2007], a few specific intervals of the magnetic field dipolarizations and reversals [*Vogt et al*., 2010], and auroral polar dawn spots thought to be the ionospheric signature of inward flow from a tail reconnection region [*Radioti et al*., 2008]. Additionally, *Kronberg et al*. [2009] reported quasiperiodic variations of the ion spectral index γ on 12 Galileo orbits with periods ranging from 1.5 to 7 days, but typically ~2.5–4 days. Magnetohydrodynamic simulations of the Jovian and Kronian magnetospheres [e.g., *Fukazawa et al*., 2005, 2006, 2010; *Zieger et al*., 2010; *Jia et al*., 2012] have shown that the timescales for periodic plasmoid release (driven by both the solar wind and internal processes) can vary with solar wind conditions at both Jupiter and Saturn. It is therefore possible that the solar wind modulates the characteristic mass loading/release period, which could explain why the strong periodicity is only observed intermittently.

The purpose of the present study is to characterize the structure and other properties of Jovian plasmoids to establish the typical length scale and duration of the observed plasmoids. This information allows us to estimate the amount of mass released and flux closed by reconnection of open field lines following a typical plasmoid event. We compare our results to estimates of the mass loading rate from Io and the rate at which flux is opened by dayside reconnection with the solar wind to determine the importance of the observed plasmoids to the overall mass and flux transport at Jupiter.

3. Methods

3.1. Magnetic Signature of Plasmoids

This study concerns the properties of plasmoids observed in magnetometer data from Jupiter's magnetotail. Plasmoids are identified by a characteristic bipolar signature in the north–south component of the magnetic

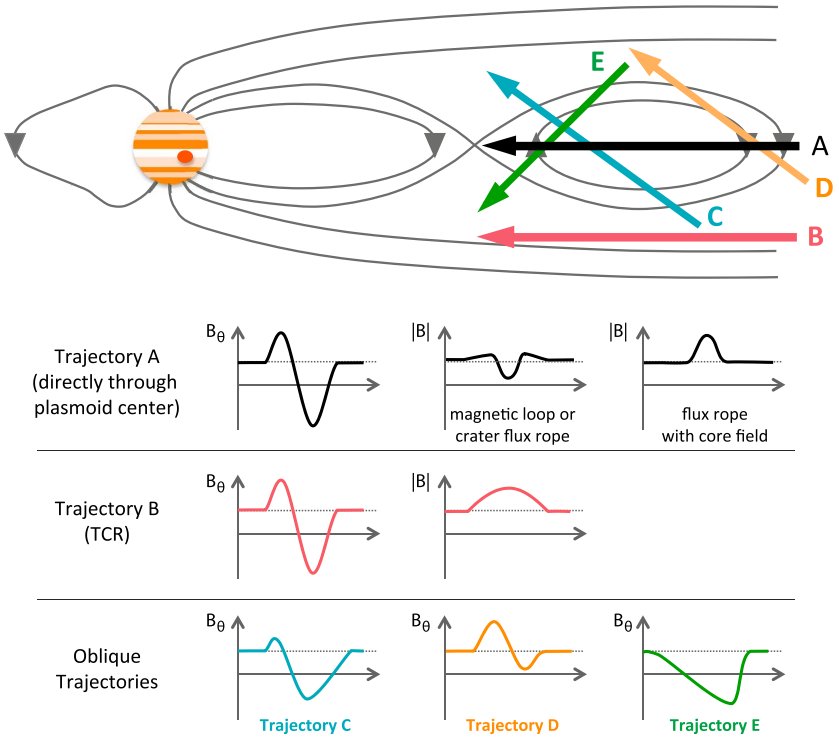

Figure 2. Schematic (not to scale) showing how the observed B_θ signature depends on the spacecraft trajectory with respect to the plasmoid. After *Borg et al.* [2012].

field [*Hones*, 1976; 1977]. The form of the north–south field signature depends on the trajectory of the plasmoid relative to the observing spacecraft, as illustrated in Figure 2. Jupiter's equatorial field is typically southward, so that the equatorial B_θ, the meridional component of the magnetic field, is positive. Therefore, for a plasmoid moving tailward with respect to a spacecraft, the spacecraft will observe an enhanced southward ($B_\theta > 0$) then northward ($B_\theta < 0$) field. In the case of a plasmoid moving planetward, the B_θ polarity will be reversed. If the spacecraft passes close to the central region of the plasmoid it will record a relatively symmetric bipolar B_θ signature, with the intervals of enhanced northward and southward fields being roughly equal in magnitude and duration (see Figure 2, trajectory A). However, if the spacecraft does not pass through the central region of the plasmoid it will record an asymmetric B_θ signature (trajectories C and E) or may not record a B_θ sign change at all (trajectory D). The plasmoid may also be detected remotely as a traveling compression region [*Slavin et al.*, 1993] in which B_θ displays the characteristic bipolar signature and a gradual increase in the field magnitude due to the compression of the lobe field as it drapes about the plasmoid (see Figure 2, trajectory B). If the spacecraft does not pass through the central region of the plasmoid it is not possible to accurately estimate the size or other properties of the plasmoid such as whether or not it has a significant core field.

Assuming the spacecraft passes close to the central region of a tailward moving plasmoid, the bipolar B_θ signature and minimum in B_θ will be followed by a return to background levels. Under the further assumption that the plasmoid's radial flow maintains a near-constant speed, the nature of this recovery can indicate whether the observed tail reconnection is occurring on open or closed field lines, as is illustrated in Figure 3. If the recovery is on the same timescale as the field dipolarization and reversal signatures so that the spacecraft records only the symmetric B_θ signature of the plasmoid, then the reconnection likely proceeded on closed field lines (Figure 3, middle row). By comparison, if reconnection proceeds onto open lobe field lines, the spacecraft will record an extended interval of negative B_θ following the main plasmoid signature (Figure 3, bottom row). This region of open lobe field lines draped over the tailward moving plasmoid, detected as the extended interval of negative B_θ, is called the postplasmoid plasma sheet, or PPPS [*Richardson et al.*, 1987]. At Jupiter, the PPPS signature may be expected for Dungey cycle reconnection, which would involve closure of open flux in the tail lobes, but not for the centrifugally driven reconnection of the Vasyliūnas cycle.

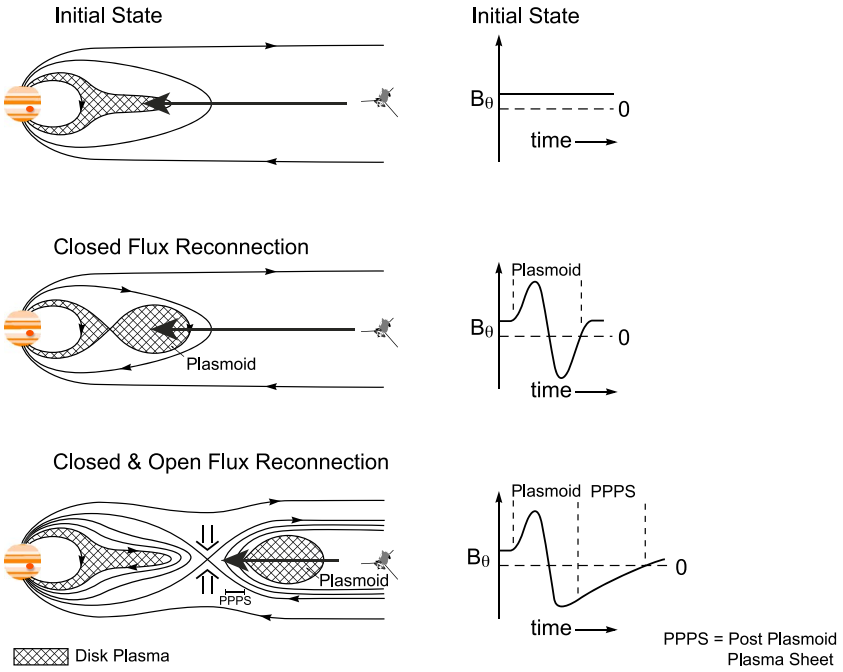

Figure 3. Schematic (not to scale) comparing the (left column) field line configuration and (right column) observed B_θ signature during (top row) quiet conditions, (middle row) closed flux reconnection, and (bottom row) open flux reconnection. The assumed spacecraft trajectory is directly through the center of the plasmoid, as indicated by solid black horizontal lines. Modified from Figure 2 of *Jackman et al.* [2011].

The magnetic field in the PPPS consists of newly reconnected field lines with both ends in the interplanetary magnetic field (IMF), so information about the PPPS duration and flow speed can be used to estimate the amount of open flux that is closed through reconnection of open lobe field lines, as we discuss in section 4.5. However, it is important to note that the PPPS interpretation assumes the spacecraft crosses near to the center of the plasmoid, such as trajectory A in Figure 2. Otherwise, if the spacecraft's trajectory is oblique, an extended interval of negative B_θ may be recorded even in the absence of any PPPS (see Figure 2, trajectory C). Additionally, if the radial velocity slows significantly as a plasmoid moves tailward, a spacecraft may record an extended interval of negative B_θ (from the planetward edge of the plasmoid) without encountering IMF lines in the PPPS. Observations from the Earth show that terrestrial plasmoids accelerate as they are pulled tailward by IMF field lines which are draped around the plasmoid [*Ieda et al.*, 1998], so the magnetic signature of a PPPS likely does indicate closure of open flux at the Earth. However, at Jupiter, Vasyliūnas cycle plasmoids would be enveloped within closed field lines which could slow the tailward plasmoid motion. Unfortunately, without high time resolution velocity measurements, it is impossible to distinguish whether the PPPS signature in Jovian plasmoids truly indicates closure of open lobe field lines or whether the plasmoid velocity slows as it moves tailward. Similarly, in the absence of high time resolution density measurements, it is not possible to determine whether reconnection during the PPPS interval is proceeding on low-density lobe field lines or high-density plasma sheet field lines. In order to place an upper limit on the amount of open flux closure that is associated with Jovian plasmoid events, in section 4.5 we calculate the amount of flux closed during a typical plasmoid event as if the plasmoid velocity remains constant so that the interval of extended B_θ occurs because of open flux closure.

3.2. Plasmoids Analyzed in This Study

The plasmoids considered in this study were selected from a set of 249 reconnection events previously studied by *Vogt et al.* [2010], who surveyed all of the nightside magnetometer data, including Pioneer 10 and 11, Voyager 1 and 2, Ulysses, and Galileo, at distances beyond 30 R_J. They identified reconnection intervals on the basis of field dipolarizations and reversals in which $|B_\theta|$ increased over background levels by at least a factor of 2 (see *Vogt et al.* [2010, section 3.2] for a complete description of the quantitative identification criteria used). The background level is defined as the 1 day running average of $|B_\theta|$, so that the background changes slowly in time but reflects large-scale variations with radial distance and local time.

We searched through the 249 *Vogt et al*. [2010] events by eye to select the clearest signatures of tailward moving plasmoids. We looked for intervals with a positive (southward) B_θ enhanced over background levels followed by a field reversal in which B_θ changes sign and turns negative (northward), with $|B_\theta|$ again enhanced over background levels. The timescale for the field reversal was required to be comparable to or shorter than the interval of enhanced $|B_\theta|$ (ignoring the PPPS, which can be significantly longer). Our search yielded 43 plasmoids found in 35 of the 249 reconnection events. (Some of the reconnection events included more than one plasmoid signature; see discussion of chain events in section 4.3.) Most of the plasmoids occurred during the 45 reconnection events that *Vogt et al*. [2010] designated as "bipolar" because B_θ changed sign during the event and was not predominantly (at least 85% of the event duration) either negative or positive. However, not all of the bipolar events met our criteria to be classified as a tailward moving plasmoid. For example, an event in which B_θ is initially negative and then turns positive would not indicate a tailward moving plasmoid, and similarly we would not select an event in which an initially southward field reverses but $|B_\theta|$ remains smaller than background levels.

3.3. Probing the Interior Structure With Minimum Variance Analysis

Plasmoids may be classified as flux ropes or closed magnetic loops based on their magnetic field topology [*Hughes and Sibeck*, 1987; *Moldwin and Hughes*, 1992; *Slavin et al*., 2003a, 2003b]. Flux ropes are helical, three-dimensional structures of twisted magnetic field which often contain a central core field along the axis of the flux rope. By comparison, magnetic loops (also called magnetic islands or "bubbles") are planar structures and lack a core field. In magnetic field measurements, a core field is identified by a local maximum in the field magnitude as the spacecraft passes near or through the center of the plasmoid, as identified by the sign change in B_θ. The absence of a core field, marked by a local minimum in the field magnitude at the center of the plasmoid, may be indicative of either a magnetic loop structure or a so-called "crater" flux rope [*Farrugia et al*., 1988]. Crater flux ropes would be expected in high β (ratio of thermal to magnetic pressure) plasmas because the increased plasma pressure at the plasmoid center reduces the field magnitude [e.g., *Kivelson and Khurana*, 1995].

Hughes and Sibeck [1987] predicted that a plasmoid core field would occur due to shearing between the lobe fields in the Earth's magnetotail from large-scale Maxwell stresses exerted by the open magnetic fields crossing the tail magnetopause. In this case, a positive correlation would be expected between the GSM-*y*, or crosstail, magnitude and direction of the core field and that of the interplanetary magnetic field, or IMF. *Moldwin and Hughes* [1992] found that the core field and IMF direction were well correlated, though more recent studies [e.g., *Slavin et al*., 2003a] have reported a weaker correlation. For the tailward moving plasmoids studied here, where the bipolar signature is in the B_θ component, we expect any core field to be orthogonal to B_θ and predominantly in the azimuthal B_φ direction.

One way to determine the flux rope or loop structure of a plasmoid is through minimum variance analysis (MVA). This approach assumes a favorable spacecraft trajectory with respect to the plasmoid and can be misleading due to temporal evolution of a flux rope structure [e.g., *Zhang et al*., 2010]. MVA involves transforming the magnetic field during the plasmoid interval into the principal axis coordinate system where the three components are along the directions of maximum, intermediate, and minimum variance [*Sonnerup and Cahill*, 1967; *Russell and Elphic*, 1978]. In this coordinate system, the flux rope magnetic field will display an elliptical rotation in the plane defined by the maximum and intermediate variance field components. MVA results from two example plasmoids are shown in sections 3.4 and 4.4.

3.4. Case Study Event on 8 March 1979

Magnetic field data for a plasmoid, observed on 8 March 1979 by Voyager 1 at a radial distance of 54 R_J and ~03:48 LT, are shown in Figure 4. (The other 42 plasmoids were identified in the Galileo magnetometer data.) No useful Voyager plasma data are available during this interval due to spacecraft pointing (F. Bagenal, personal communication, 2012). The $|B_\theta|$ values recorded during this plasmoid are among the largest observed in any of the plasmoid events: from background levels of ~1 nT, B_θ reached a maximum of ~11 nT and a minimum of roughly -7 nT. We define the plasmoid duration as the time between the maximum and minimum B_θ values, excluding the B_θ recovery or postplasmoid plasma sheet; by this definition the plasmoid lasts for ~3.4 min. Following the minimum, B_θ remains negative for just under 5 min. The B_θ signature during this plasmoid is relatively symmetric and does not display evidence of an extended PPPS.

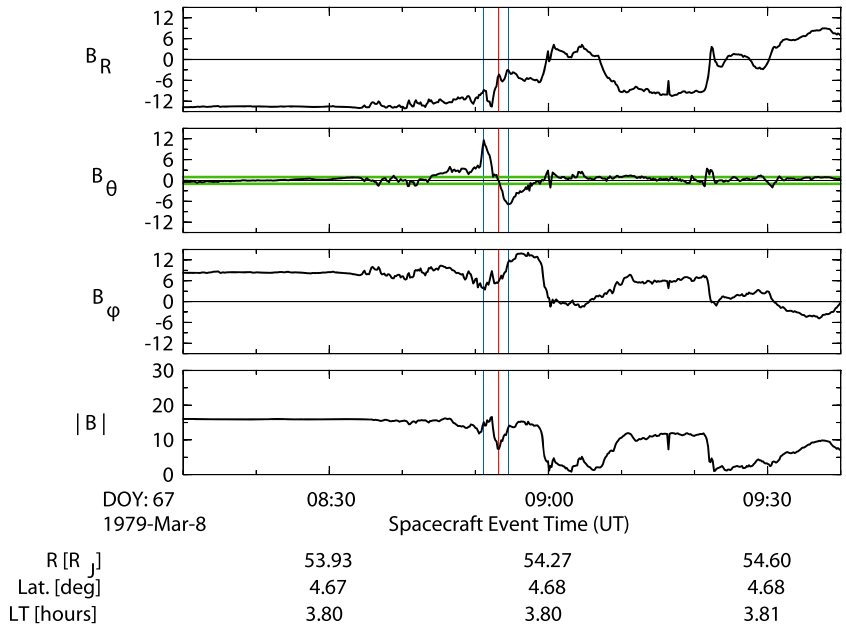

Figure 4. Voyager 1 magnetic field data in System III coordinates from a plasmoid event on 8 March 1979. The magnetic field is in units of nT. The vertical blue lines indicate the plasmoid start and end times, and the vertical red line indicates the plasmoid center. The horizontal green lines in the third panel indicate the magnitude of the background B_θ, defined as the 1 day running average of $|B_\theta|$.

The structure of this plasmoid is consistent with a magnetic loop rather than a flux rope. The magnitude of B_R, the radial component of the magnetic field, decreases just before the zero crossing in B_θ, and the field magnitude reaches a local minimum at the time of the B_θ zero crossing (red vertical dashed line), suggesting a magnetic loop structure or possibly a crater flux rope. Figure 5 shows the magnetic field in both System III and minimum variance coordinates, as well as hodograms for the plasmoid interval. In the minimum variance coordinate system, B_1 is along the direction of the maximum variance, B_3 is along the direction of the minimum variance, and B_2 is in the intermediate direction. We performed the MVA over the plasmoid interval as defined by the B_θ peaks, or the maximum and minimum B_θ values, indicated in Figure 4 by the vertical blue lines. (Shifting the MVA window by a few time steps in either direction did not appreciably affect the result.) If the plasmoid had a flux rope structure, we would expect a rotation in an elliptical arc in the plane defined by the maximum (B_1) and intermediate (B_2) eigenvectors, but this is not seen in the hodogram in Figure 5. Eigenvectors show that the field in the direction of maximum variance, B_1, is aligned primarily in the north–south direction; the field in the direction of minimum variance, B_3, is primarily in the azimuthal direction; and the intermediate field, B_2, is primarily in the radial direction as expected for a simple loop structure.

4. Results: Plasmoid Statistical Properties

From the initial *Vogt et al*. [2010] list of 249 reconnection signatures in the magnetometer data, we identified 43 tailward moving plasmoid events characterized by a bipolar B_θ signature as described in section 3.1. Table 1 summarizes the key properties of the events, including their location, duration, B_θ amplitude, magnetic flux closed, and presence or absence of a core field. In the following subsections we discuss the average properties and structure in more detail and present a superposed epoch analysis of the 43 plasmoid events.

4.1. Plasmoid Distribution in Radial Distance and Local Time

Figure 6 shows the distribution of the 43 plasmoids in the Jovigraphic equatorial plane, along with the spacecraft orbits, location of the *Vogt et al*. [2010] statistical X-line, and the positions of the remaining 214 reconnection events identified in the magnetometer data for reference. Most of the data from the Galileo spacecraft were taken from near the Jovigraphic equator, and as a result, all but two of the plasmoids are

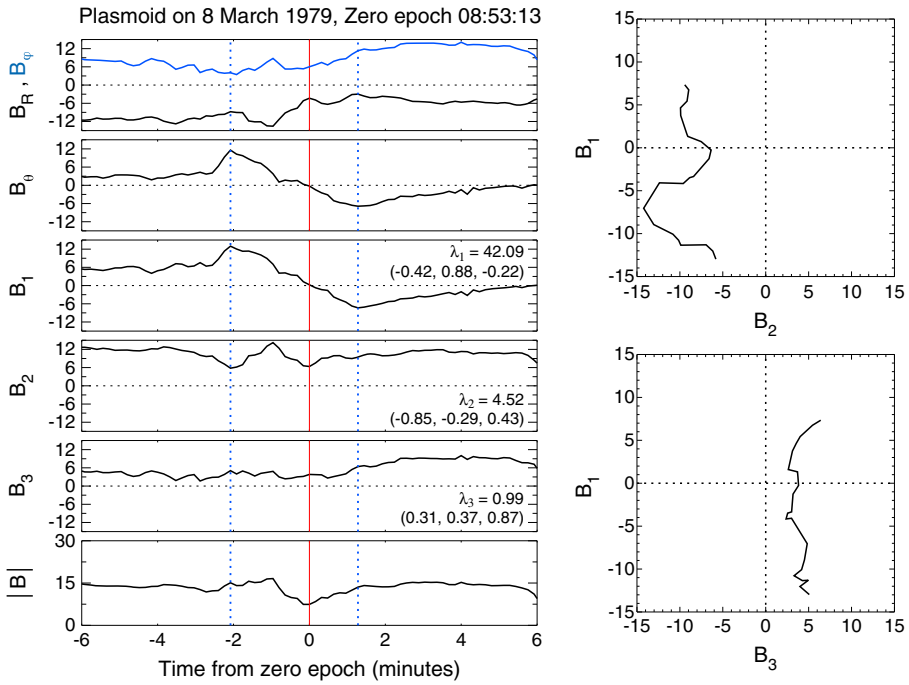

Figure 5. (left) Magnetic field data from the plasmoid event on 8 March 1979, in (first and second panels) System III coordinates, (third to fifth panels) rotated into minimum variance coordinates, and (sixth panel) the field magnitude. In the first panel, B_R is drawn in black and B_φ is drawn in blue. The plasmoid interval is indicated by the vertical dashed blue lines and the plasmoid center by the vertical red solid line. Eigenvectors, which give the directions of the orthogonal unit vectors from the minimum variance analysis in System III (R,θ,φ) coordinates, and eigenvalues are provided in the third to fifth panels. (right) Hodograms showing the maximum (B_1) versus intermediate (B_2) variance components and the maximum (B_1) versus minimum (B_3) variance components.

located within 2 R_J of the Jovigraphic equator; the other two plasmoids were observed during Voyager 1 and Galileo orbit G1, at ~5° latitude. All plasmoids were observed within 9 R_J of the magnetic equator.

Perhaps the most striking feature of the plasmoid distribution in Figure 6 is that all but one of the plasmoids are found at postmidnight local times, with most between 01:30 and 03:00 LT. A histogram of the local time distribution is shown in Figure 7. The plasmoids are also relatively constrained in radial distance, as can be seen in the histogram of radial distance in Figure 7. The number of observed plasmoids peaks between 95 and 100 R_J, just beyond the statistical X-line at ~90 R_J. By comparison, the *Vogt et al.* [2010] reconnection events were observed across all nightside local times and span ~30–150 R_J in radial distance. Like the 43 plasmoids identified here, the full set of reconnection events is not evenly distributed in local time, with more events postmidnight than premidnight. However, the frequency of reconnection events can be shown to be roughly equal on either side of midnight because there is a significant difference in the amount of data available in the two local time sectors.

4.2. Plasmoid Duration and Length Scale

We define the plasmoid duration as the time between the maximum and minimum B_θ, or the peak southward and northward field, following *Slavin et al.* [1993]. Using this definition, the mean duration of the 43 plasmoids is 6.8 min. Figure 7 shows a histogram of the duration for each plasmoid, and the values are also listed in Table 1. The plasmoid length can be found by multiplying the plasmoid radial velocity by the duration of the plasmoid. We must use an average value for V_R because of the velocity measurements' low time resolution (3–11 min) compared to the mean duration of ~7 min, so it is impractical to consider individual data points in our calculation. Instead, we take a typical plasmoid radial velocity in the plasma sheet, ~450 km/s [*Kronberg et al.*, 2008a], and multiply by the plasmoid duration, which produces an average plasmoid length of ~2.6 R_J. This radial velocity assumption is probably an oversimplification, as we would not expect each plasmoid to move outward with the same velocity, nor for the velocity to remain constant for the duration of the plasmoid.

Journal of Geophysical Research: Space Physics
10.1002/2013JA019393

Table 1. Times and Properties of the 43 Plasmoids Used in This Study

Date	Start Time	End Time	Duration (min)	PPPS Duration to B_θ Zero Crossing (min)	PPPS Duration to B_θ Background (min)	Max. B_θ (nT)	Min. B_θ (nT)	Latitude (deg)	Longitude (deg)	Radial Distance (R_J)	Local Time	Flux Closed PPPS B_θ Zero[a] (GWb)	Flux Closed PPPS B_θ Background[a] (GWb)	Core Field
1979 Mar 08	08:51:08	08:54:30	3.36	4.64	3.04	11.6	−6.88	4.68	249.76	54.19	3.8	*1.06*	*0.98*	No
1996 Aug 13	21:18:14	21:23:02	4.8	15.6	2.4	2.36	−2.25	−4.26	25.33	119.67	3.96	1.74	0.25	No
1996 Sep 20	13:22:27	13:28:51	6.4	1.6	1.2	2.96	−3.42	−0.51	325.61	86.81	1.93	*0.25*	*0.20*	No
1996 Sep 20	18:44:03	18:46:27	2.4	10.8	1.2	2.14	−2.12	−0.51	132.3	87.54	1.96	1.84	0.12	No
1996 Sep 20	19:12:51	19:20:51	8	32.8	31.2	2.4	−8.84	−0.51	113.23	87.62	1.96	12.09	12.01	No
1996 Sep 23	00:34:51	00:38:27	3.6	6.4	6	2.42	−4.32	−0.52	342.4	94.24	2.18	*0.99*	*0.98*	No
1996 Sep 24	08:12:03	08:24:51	12.8	24	23.2	3.2	−4.11	−0.53	273.2	97.64	2.29	*4.96*	*4.95*	No
1996 Sep 24	08:52:03	08:53:39	1.6	60	5.2	1.06	−6.36	−0.53	253.65	97.69	2.3	16.40	1.54	No
1996 Sep 25	00:43:39	00:52:27	8.8	4.4	3.2	1.77	−2.74	−0.53	36.83	99.25	2.35	*0.36*	*0.33*	No
1996 Sep 26	09:21:39	09:30:27	8.8	9.6	9.6	1.51	−7.1	−0.53	296.32	102.14	2.46	*4.64*	*4.64*	No
1996 Sep 26	09:40:27	09:46:03	5.6	142	26.4	4.97	−7.26	−0.53	285.69	102.17	2.46	23.84	8.83	No
1996 Sep 28	19:55:39	20:19:39	24	6	6	4.2	−6.44	−0.54	326.64	106.44	2.64	*2.39*	*2.39*	No
1996 Sep 28	20:55:39	21:00:27	4.8	40.4	38	1.68	−8.54	−0.54	299.11	106.48	2.64	15.96	15.82	No
1996 Sep 30	23:52:51	00:06:27	13.6	10.8	5.6	1.68	−2.96	−0.54	251.08	109.29	2.78	*1.11*	*0.84*	No
1996 Oct 01	17:02:03	17:08:03	6	4.8	4	3.97	−5.23	−0.54	350.86	110.04	2.83	*1.02*	*1.00*	No
1996 Oct 03	16:41:39	16:50:03	8.4	4.8	4.4	3.71	−2.71	−0.54	62.02	111.69	2.96	*0.62*	*0.61*	No
1996 Oct 05	09:44:27	09:54:27	10	7.6	5.2	2.81	−3.34	−0.54	16.84	112.56	3.06	*1.28*	*1.04*	Yes
1996 Oct 05	10:02:27	10:06:51	4.4	221.2	123.6	2.69	−5.09	−0.54	6.21	112.56	3.06	31.07	26.63	No
1996 Oct 12	02:23:14	02:30:50	7.6	9.2	8.4	2.57	−3.4	−0.54	315.87	111.23	3.48	*1.34*	*1.33*	No
1996 Oct 15	16:00:02	16:05:38	5.6	4	1.2	1.86	−2.73	−0.53	95.74	107.37	3.71	*0.32*	*0.11*	Yes
1996 Oct 18	17:08:26	17:14:26	6	7.6	7.2	2.49	−3.72	−0.53	326.09	102.22	3.93	*1.13*	*1.13*	No
1996 Oct 18	18:18:26	18:20:26	2	56.4	2.8	1.73	−2.73	−0.53	284.56	102.13	3.94	1.91	0.29	No
1996 Oct 20	10:09:14	10:14:26	5.2	52.8	1.2	3.13	−3.13	−0.52	280.61	98.52	4.07	4.47	0.18	No
1996 Oct 20	12:39:38	12:43:14	3.6	15.6	12.4	2.25	−4.7	−0.52	190.79	98.28	4.08	2.56	2.42	Yes
1997 Apr 13	04:16:40	04:30:40	14	2.4	2.4	3.86	−4.75	−1.31	32.32	63.03	0.73	*0.63*	*0.63*	No
1997 Apr 16	07:01:52	07:06:40	4.8	3.6	2.4	5.48	−1.62	−1.39	210.77	71.03	1.24	*0.26*	*0.24*	No
1997 Aug 03	02:25:04	02:31:28	6.4	28.8	15.2	1.44	−2.16	−0.21	162.78	141.61	0.15	1.20	1.05	No
1997 Jun 05	00:10:15	00:13:51	3.6	30.8	30.8	2.27	−3.49	−0.42	141.91	99.56	1.53	7.58	7.58	No
1997 Jun 07	04:40:39	04:49:03	8.4	26.8	26.8	5.28	−6.78	−0.42	39.1	97.86	1.7	10.94	10.94	No
1997 Jun 10	11:37:26	11:39:02	1.6	36	21.6	4.92	−3.94	−0.41	61.52	93.29	1.96	7.87	5.82	No
1997 Jun 14	00:59:02	01:07:50	8.8	26.4	16	2.45	−6.76	−0.4	210.15	85.35	2.3	7.17	4.96	No
1997 Jun 14	01:34:14	01:39:50	5.6	64.8	45.6	2.9	−13.44	−0.4	189.64	85.29	2.3	23.08	20.41	No
1997 Jun 14	13:16:14	13:20:38	4.4	4	0.8	2.79	−2.29	−0.4	124.62	83.92	2.35	*0.48*	*0.08*	No
1997 Jun 14	13:36:38	13:44:38	8	4.4	4	5.23	−3.89	−0.4	111.1	83.88	2.35	*0.73*	*0.71*	Yes
1997 Jun 19	14:28:14	14:31:26	3.2	19.6	19.2	1.65	−5.1	−0.37	60.69	65.27	3.05	4.08	4.05	No
1997 Jun 21	02:34:14	02:39:02	4.8	72.4	29.6	3.77	−4.17	−0.35	195.07	57.71	3.35	8.27	6.51	No
1997 Mar 19	18:40:36	18:44:36	4	30.8	20.8	1.71	−3.27	0.17	66.47	84.96	2.88	4.24	3.61	No
1997 May 30	13:39:51	13:54:39	14.8	4.8	4.8	3.02	−2.25	−0.42	185.05	99.29	1.13	*0.67*	*0.67*	No
1997 Oct 13	17:49:03	18:08:15	19.2	4.4	4	2.43	−4.49	0.11	84.78	98.92	0.62	*0.81*	*0.81*	No
1997 Oct 13	18:23:03	18:32:15	9.2	3.2	1.6	1.78	−3.06	0.11	69.33	98.92	0.62	*0.28*	*0.20*	No
1997 Oct 21	16:55:03	16:56:39	1.6	17.6	14.8	1.9	−5.17	0.06	9.42	91.38	1.25	2.52	2.44	No
1997 Oct 29	08:34:14	08:36:14	2	3.2	3.2	1.68	−2.7	−0.06	201.87	68.45	2.14	*0.33*	*0.33*	No
1999 Oct 24	04:29:17	04:32:53	3.6	24	0.4	6.31	−3.78	0.01	265.93	85.59	20.12	7.38	0.11	No
Average			6.87	27.00	13.88	3.07	−4.49			94.72	2.85	5.16	3.72	
Superposed epoch analysis			6.40	45.00	128.00	1.40	−3.40					8.80	6.20	

[a]Flux closure values assume a 45 R_J azimuthal plasmoid width. Numbers listed in italics indicate plasmoids for which the PPPS duration is less than twice the plasmoid duration.

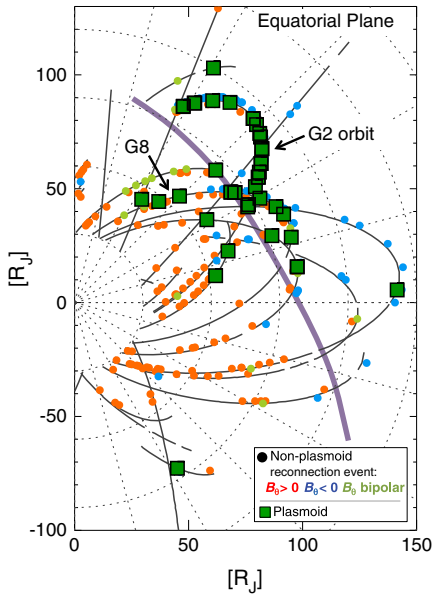

Figure 6. Distribution of tailward moving plasmoids (green squares) in Jupiter's nightside magnetosphere. Also shown are the locations of other observed reconnection signatures (colored dots, where color indicates the dominant sign of B_θ during the event), the *Vogt et al.* [2010] statistical X-line (purple line), and spacecraft orbits (solid black lines). This is a Jovigraphic equatorial plane view, and the Sun is to the left. Spacecraft orbits are represented by solid black lines.

Our average plasmoid duration, and therefore also the calculated plasmoid length, is shorter than the ~10–20 min duration and ~9 R_J length found by *Kronberg et al.* [2008a] because they defined the plasmoid duration as the interval starting when B_θ, which is positive/southward, becomes enhanced, and ending when the northward or negative B_θ returns to zero. Using their definition, rather than the maximum and minimum B_θ, the average duration of the 43 plasmoids from this study would be 39 min with a corresponding length of 14.7 R_J, again assuming a constant 450 km/s outward velocity. However, the Kronberg et al. definition includes the postplasmoid plasma sheet as part of the plasmoid interval, which is inappropriate for our use because it would result in inaccurate estimates of the typical plasmoid length and mass released. We therefore follow the *Slavin et al.* [1993] definition, recognizing, as those authors did, that using the interval between the maximum and minimum B_θ underestimates the plasmoid size. The force-free flux rope model of *Kivelson and Khurana* [1995] predicts that the maximum in a plasmoid's B_z signature (comparable to B_θ) occurs at $\pm L \sin^{-1}((1+\varepsilon^2)^{-1/2})$ from the plasmoid center, where the plasmoid length is $2\pi L$ and ε is the amplitude of the B_z perturbation relative to the background lobe field. This means that, for typical values of ε from 0 to 1, our definition of the plasmoid interval may underestimate the plasmoid size by a factor of ~4–8, and a typical plasmoid length could be as large as ~10–20 R_J.

4.3. Recurrence Time and Chain Events

"Chain" events, or groups of plasmoids separated in time by about one hour, are common when plasmoids are observed at the Earth [cf. *Moldwin and Hughes*, 1992; *Slavin et al.*, 1993], Saturn [*Jackman et al.*, 2011], and Mercury [*Slavin et al.*, 2012]. At Saturn, the chains are interpreted as a series of plasmoids originating from a single reconnection region. Nearly half (18 of 43) of the Jovian plasmoids are found to occur in groups or chains of two plasmoids separated by 90 min or less, though most were separated by less than an hour. An example of such a chain, on 18 October 1996 during Galileo orbit G2, is given in Figure 8, where the plasmoids are marked by vertical lines. The first plasmoid begins at 17:08 UT and lasts for 6 min and is followed by a second, smaller—in both duration and amplitude—plasmoid at 18:18 UT.

A good estimate of the average plasmoid production rate is crucial to calculating the mass loss and flux closure rates, which we discuss in section 5.1. However, identifying a "typical" plasmoid recurrence time is difficult. Most plasmoids were observed during just three of the more than 30 Galileo orbits: G2 in September to October 1996 (22 plasmoids), G8 in May to June 1997 (10 plasmoids), and C10 in October 1997 (4 plasmoids). With the exception of the chain events, the average time between plasmoids was 2–3 days for G2 and G8 and 8 days during C10. So while we can conclude that the recurrence time during these active orbits is a few days, it may not be indicative of the typical plasmoid production rate, since active orbits in which plasmoids are observed are separated by several months. It is also important to consider the additional 214 non-plasmoid reconnection events that have been identified in magnetometer data [*Vogt et al.*, 2010] and not just the 43 plasmoids studied here. Though these events do not display the classic bipolar B_θ signature of a tailward moving plasmoid, it is likely that they represent the remote detection of a nearby plasmoid and should therefore be considered when estimating the average plasmoid production rate. The reconnection events are typically observed with recurrence times of a couple of days and frequently appear in groups of two [e.g., *Vogt et al.*, 2010, Figure 12].

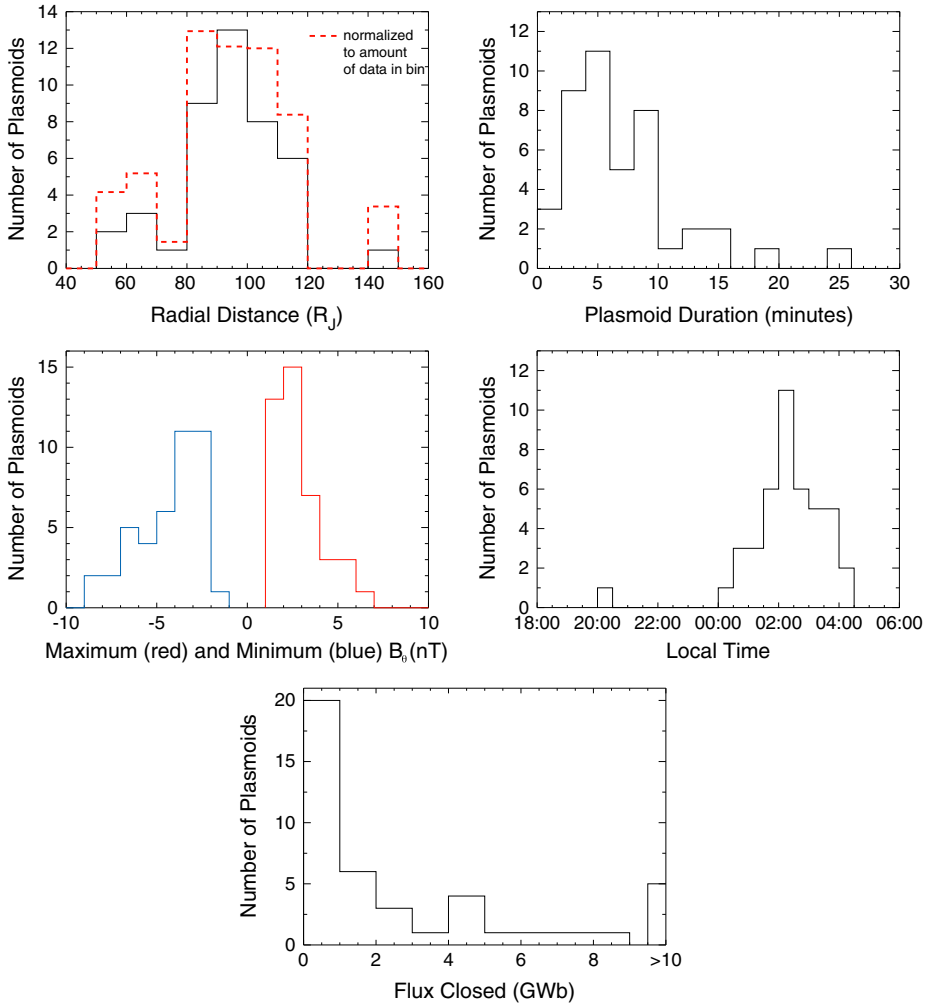

Figure 7. Histograms of various plasmoid properties. For the calculated flux closure the assumed plasmoid azimuthal width is 45 R_J.

In the absence of simultaneous multipoint measurements or information about upstream solar wind conditions, it is impossible to determine whether the magnetosphere was especially dynamic at the times of the active orbits due to external solar wind conditions, or whether the active orbits took the spacecraft through an especially dynamic region of the magnetosphere. In the former case, the long-term typical recurrence time would be weeks or longer, considering only 241 reconnection events (including 42 clear plasmoid examples) were observed in Galileo magnetometer data [*Vogt et al.*, 2010]. By comparison, in the latter case, the typical plasmoid production timescale would be just 2–3 days, though a spacecraft would only observe plasmoids or other reconnection signatures when it passed through a certain region of the magnetosphere (for example, 80–110 R_J, 01:30–03:00 local time). Since plasmoids and the nonplasmoid reconnection events are often observed in pairs the average plasmoid production rate could even be as high as one plasmoid per day.

4.4. Minimum Variance Analysis

Only 4 of 43 plasmoids display an increase in the field magnitude at the time of the B_θ zero crossing which would indicate an azimuthal core field and flux rope-like structure. The remaining plasmoids are therefore likely to be magnetic loops or possibly crater flux ropes, though it is possible that the plasmoid trajectories relative to the spacecraft missed the central region of the structure and, therefore, did not encounter a core field that would be present in a classic flux rope. Ideally, minimum variance analysis would also be performed on each plasmoid to examine the internal structure, but the time resolution of the magnetometer data, one vector per 24 s, is too low for MVA to be a useful tool for most of our cases. As the histogram in Figure 7 shows,

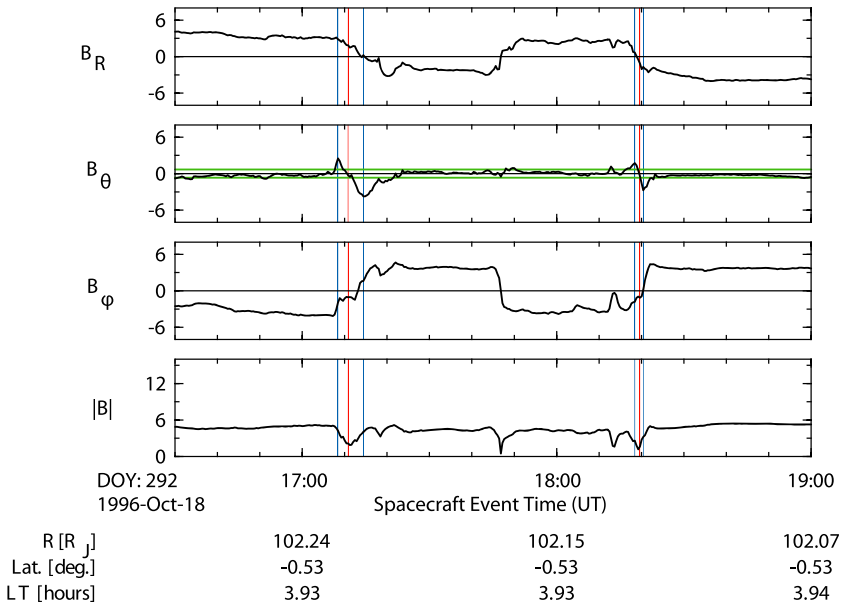

Figure 8. Magnetic field data from a chain of plasmoids observed on 18 October 1996, during Galileo orbit G2. Format as in Figure 4.

most plasmoids last less than 6 min, meaning there would typically be only 15 data points or fewer for the MVA. We have, however, performed the MVA for the four cases in which we observe a core field, to further test whether these plasmoids show evidence of a flux rope structure. Results for one of the plasmoids are shown in Figure 9. Hodograms for two of the other plasmoids are inconclusive, due in part to their short duration (~6 min).

Of the four plasmoids with a core field, the plasmoid at 13:36 UT on 14 June 1997, seen in Figure 9, is the most likely flux rope candidate based on the hodograms; there is a partial arc rotation in the plane defined by the

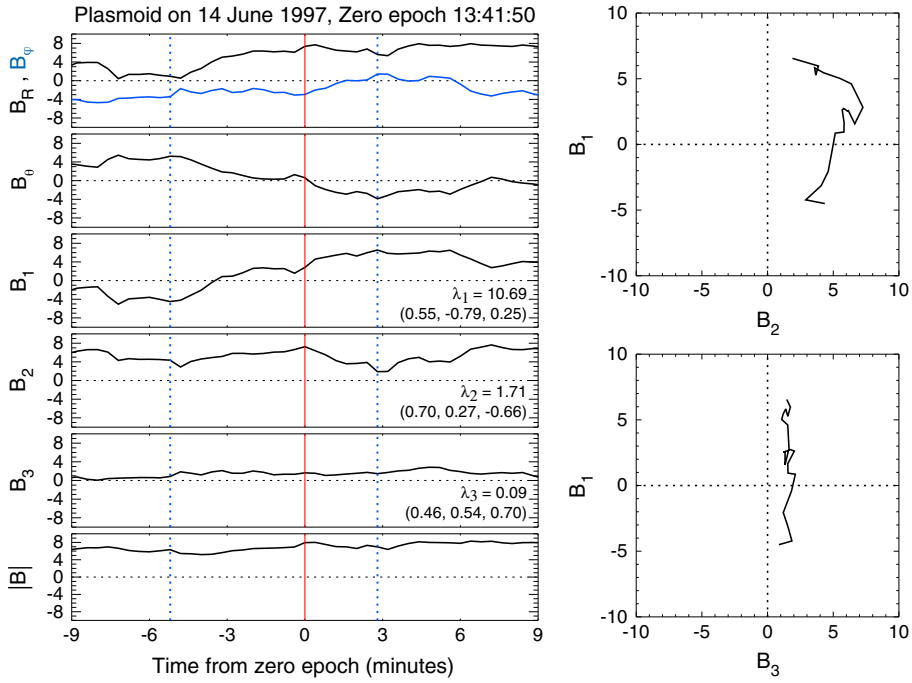

Figure 9. (left) Magnetic field data and (right) hodograms for a plasmoid on 14 June 1997, following the format of Figure 5.

maximum (B_1) and intermediate (B_2) eigenvectors. This plasmoid had a duration of 8 min. The MVA shown in Figure 9 was performed over the plasmoid interval as defined by the B_θ peaks, since tests showed that shifting the MVA window by a few time steps in either direction did not appreciably affect the result.

4.5. Flux Closed During a Typical Plasmoid Event

In order to understand the role of plasmoids in the overall flux transport at Jupiter, we can calculate the average amount of open flux closed via reconnection of open field lines in the postplasmoid plasma sheet, as discussed in section 3.1, during a typical plasmoid event to then determine the rate of flux closure. The amount of open flux Φ closed in the postplasmoid plasma sheet is given by

$$\Phi = L_\varphi \int V_R B_\theta dt, \quad (1)$$

where L_φ is the plasmoid's azimuthal width, V_R is the outward radial velocity, and the integral is taken over the duration of the PPPS [cf. *Jackman et al*., 2011]. This calculation requires several assumptions. First, we assume that the interval of extended negative B_θ is produced by reconnection of open (lobe) field lines and is not the result of spacecraft trajectory effects or by a decrease in plasmoid velocity as it moves tailward (see discussion in section 3.1). Second, we must use an average value for V_R for the reasons outlined in section 4.2 where we calculate the plasmoid radial extent and again use the ~450 km/s velocity reported by *Kronberg et al*. [2008a].

We must also make an assumption about the plasmoid's azimuthal width, which is unconstrained due to the lack of multipoint measurements. An upper limit for the plasmoid azimuthal extent would be the full magnetotail width at an antisunward distance of 90 R_J, which is ~240–340 R_J depending on solar wind conditions according to the magnetopause model of *Joy et al*. [2002]. However, polar auroral spots that are thought to be associated with inward flow from reconnection [e.g., *Radioti et al*., 2008] are relatively localized, and when mapped to the magnetosphere, each spot covers an area approximately 20 R_J wide (A. Radioti, personal communication, 2013). The measured flow channel width of the reconnection events is only ~15–20 R_J [*Vogt et al*., 2010]. It is therefore likely that the plasmoids will be relatively limited in their azimuthal extent rather than extending across the tail.

Further constraints on the plasmoids' azimuthal extent can be inferred from their spatial distribution in the tail. We note that Galileo observed 24 plasmoids with a characteristic recurrence period of ~2–3 days throughout the G2 orbit, during which time the spacecraft traversed ~2 h of local time at distances beyond ~90 R_J. The rate at which plasmoids are observed (one plasmoid every 2–3 days) suggests two possibilities: Either the plasmoids' azimuthal extent covers the full ~2 h of local time covered during the G2 orbit and the plasmoid production rate is the observed one plasmoid per 2–3 days, or the azimuthal extent is more restricted but the plasmoid production rate is higher. We will assume the former case, or that the plasmoids' azimuthal extent is at least 2 h of local time at a radial distance of 90 R_J, or 45 R_J wide; this assumption affects our calculation of the amount of flux closed by a typical plasmoid but not the calculated rate of flux closure. (The rate of flux closure is the average amount of flux closed by each plasmoid multiplied by the plasmoid production rate, and if we used a smaller value for the plasmoid azimuthal extent we would use a larger value for the plasmoid production rate.) Using similar reasoning and the fact that nearly all plasmoids were observed between 01:00 and 04:00 LT and at a mean radial distance of ~90 R_J (see Figure 6), we obtain a slightly larger estimated plasmoid width, ~70 R_J.

Under the above assumptions, we calculated the flux closed during the PPPS for each plasmoid. We note that although we performed the calculation for each plasmoid, only about half (21 of 43) of the plasmoids displayed an extended PPPS, lasting at least twice as long as the plasmoid duration, which would indicate reconnection of open field lines. This would suggest that the remaining 22 plasmoids resulted from reconnection of closed field lines. In both Figure 7 and Table 1, we show two different values for the amount of flux closed. In one case, we assume that the PPPS ends when $|B_\theta|$ returns to background levels, defined as the 1 day running average of $|B_\theta|$, though B_θ remains negative, and in the other case, we assume the PPPS ends when B_θ returns to zero. In both cases the PPPS start is taken as the minimum in B_θ and we have assumed a plasmoid azimuthal width of 45 R_J. Though the B_θ zero crossing endpoint is more appropriate for most events, there are several plasmoids for which B_θ reaches its minimum value then increases to near zero within a few minutes, but remains negative (and smaller in magnitude than background levels) for tens of minutes (and in two cases longer than an hour). For these latter cases, the end of the PPPS would be best defined by the time when $|B_\theta|$ returns to background levels. Using the $|B_\theta|$ background level endpoint, the average PPPS

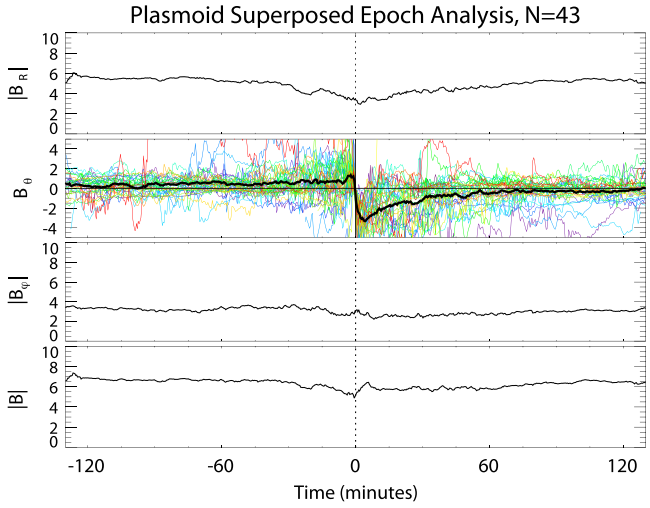

Figure 10. Superposed epoch analysis of the 43 plasmoids identified in this study (black traces). The vertical black line indicates the plasmoid center at the zero epoch, which is the time at which B_θ changes sign from positive (southward) to negative (northward). The colored lines in the second panel show B_θ data from each of the 43 plasmoids included in the superposed epoch.

duration is 14 min, and the average flux closed is ~3.7–5.8 GWb, assuming the plasmoid azimuth width ranges from 45 to 70 R_J. Similarly, using the B_θ zero crossing endpoint, the average PPPS duration is 27 min, and the average flux closed is ~5.2–8.1 GWb. This is roughly 1% of the ~720 GWb of open flux in the polar cap and tail lobes [*Vogt et al.*, 2011].

4.6. Superposed Epoch Analysis

In addition to compiling statistics on the average plasmoid properties, we performed a superposed epoch analysis, the results of which are plotted in Figure 10. Combining all 43 plasmoids into a superposed epoch analysis helps to average out effects due to the spacecraft trajectory with respect to the center of the plasmoid, and provides a way to study the typical plasmoid structure. In Figure 10 we have plotted the superposed epoch of the magnitude of the radial and azimuthal field components, to remove effects of the sign change which occurs every ~5 h as the plasma sheet moves over the spacecraft due to Jupiter's 10° dipole tilt. The zero epoch is the plasmoid center, or the B_θ zero crossing time. For plasmoid "chain" events, we split the interval between the two plasmoids so that the first half of the interval is included in the superposed epoch after the first plasmoid and the second half of the interval is used in the superposed epoch before the second plasmoid.

The superposed $|B_R|$ signature displays a gradual decrease from a background field of ~5.5 nT to ~2.9 nT just after the zero epoch. This may suggest that the spacecraft typically does not pass through the plasmoid center, as we would therefore expect a larger relative decrease in $|B_R|$. According to the force-free flux rope model of *Kivelson and Khurana* [1995], the fact that $|B_R|$ decreases by only ~50% from background levels means that the spacecraft could be as far as ~30% of the plasmoid height away from the plasmoid center. However, we note that in more than half of the plasmoids (23 of 43), B_R changed sign within 10 min of the zero epoch, and in 31 of 43 plasmoids, $|B_R|$ reached values smaller than 1 nT within 10 min of the zero epoch. It would therefore appear that the averaging of $|B_R|$ has smeared out the minimum in $|B_R|$ from each individual plasmoid because the minima do not occur precisely at the zero epoch time.

The superposed B_θ signature is initially southward, with a background value of ~0.5 nT, though the field becomes increasingly dipolar before the zero epoch. The superposed B_θ signature of the plasmoid is asymmetric, with a maximum value of 1.4 nT at 2.2 min before the zero epoch, and a minimum value of -3.4 nT at 4.2 min after the zero epoch. There is an extended PPPS and B_θ remains negative for ~128 min, though $|B_\theta|$ returns to background levels ($|B_\theta| < 0.5$ nT) after just ~45 min.

The superposed epoch does not show any evidence of a core field, as the field magnitude reaches a minimum at the zero epoch and there is no peak in $|B_\varphi|$. *Jackman et al.* [2011] reported similar signatures in the superposed epoch analysis of plasmoids at Saturn. The lack of a peak in the superposed $|B_\varphi|$ or $|B|$ signatures is

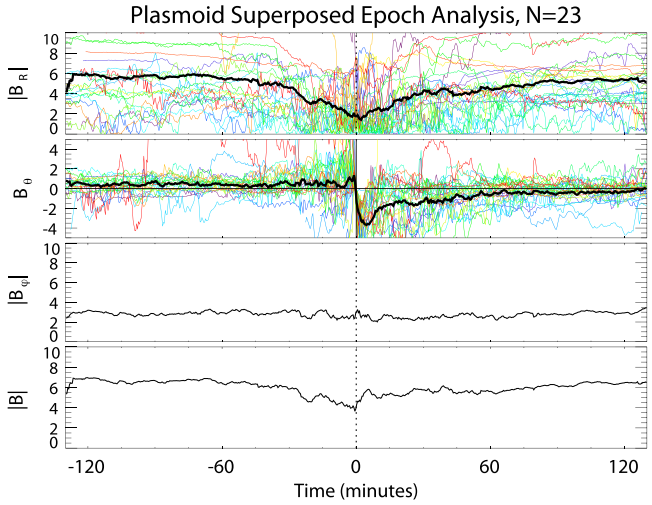

Figure 11. Superposed epoch analysis of the 23 plasmoids in which B_R changed sign within 10 min of the zero epoch, following the format of Figure 10. The colored lines in the first panel show B_R data from each of the 31 plasmoids included in the superposed epoch.

unlikely to be an effect of the averaging, as visual inspection of the 43 individual plasmoids also did not show a core field in most plasmoids. The absence of a core field or peak in $|B_\varphi|$ is also unlikely to be the result of the spacecraft's trajectory missing the plasmoid center. For example, Figure 11 shows a superposed epoch analysis of the 23 plasmoids in which B_R changed sign within 10 min of the zero epoch, suggesting that the spacecraft came close to the plasmoid center. The superposed field magnitude of these 23 plasmoids reaches a minimum at the zero epoch and the superposed $|B_\varphi|$ remains relatively constant, with no central peak near the zero epoch, similar to the superposed epoch analysis of all 43 plasmoids shown in Figure 10.

Overall, the duration and inferred size of Jovian plasmoids inferred from the superposed epoch traces in Figure 10 are similar to the properties inferred from average values of the 43 plasmoids. The average plasmoid duration (defined by the interval between the maximum and minimum B_θ) is 6.8 min, and the duration of the plasmoid signature in the superposed epoch analysis is 6.4 min. Assuming a plasmoid velocity of ~450 km/s [*Kronberg et al.*, 2008a], these durations correspond to an average plasmoid length of ~2.6 R_J and 2.4 R_J for the superposed epoch plasmoid signature. There is, however, a significant difference between the average PPPS duration seen in the 43 plasmoids, which ranges from 14 to 27 min (depending on the PPPS definition), and the PPPS duration of the superposed epoch, which is 45 to 128 min. The corresponding amount of flux closed is 6.2–13.7 GWb (depending on the PPPS definition and assumed plasmoid azimuthal width) for the superposed epoch, but the average value for the 43 plasmoids is only 3.7–8.1 GWb.

5. Discussion

5.1. Role of Plasmoids in Mass and Flux Transport at Jupiter

The average plasmoid properties described in section 4 can provide insight into the role plasmoids have in the overall transport of mass and magnetic flux in Jupiter's magnetosphere. The major source of plasma in Jupiter's magnetosphere is the volcanically active moon Io. The plasma production rate is an estimated 500–1000 kg/s on average but can vary from 260 to 1400 kg/s [e.g., *Thomas et al.*, 2004; *Bagenal and Delamere*, 2011 and references therein]. By comparison, the solar wind is a minor source of plasma, providing ~20–100 kg/s [*Hill et al.*, 1983]. On long timescales, this input must be balanced by plasmoid release and/or other mass loss processes. Therefore, we would like to calculate the mass loss rate via plasmoid release for comparison with the 500–1000 kg/s input from Io.

The mass loss rate via plasmoid release is given by the mass enclosed within a typical plasmoid, which is calculated by multiplying the plasmoid volume by the typical plasma density, divided by the plasmoid occurrence rate. In a previous calculation, *Bagenal* [2007] assumed the plasmoid was a disk with radius 25 R_J and 10 R_J height and took the density as 0.01 particles/cm^3, assuming each particle had a mass of 20 proton masses (consistent with sulfur and oxygen). The mass of each plasmoid was then ~2.4×10^6 kg, and using an

Table 2. Plasmoid Size and Mass Calculations

	Bagenal [2007]	*Kronberg et al.* [2008b]	This Study
Plasmoid length (R_J)	50 (cylinder diameter)	9	2.6–20
Plasmoid azimuthal width (R_J)	50 (cylinder diameter)	200	45–70
Plasmoid height (R_J)	10	2	2–12
Number density (/cm^3)	0.01 (particle mass 20 m_p)	0.025 (particle mass 16 m_p)	0.01 (particle mass 20 m_p)
Plasmoid mass (tons; 1 ton = 1000 kg)	~2400	~800	~28–2120
Frequency	1 plasmoid/day	Not specified	2–5 plasmoids/day
Mass loss rate	~30 kg/s	Not specified	0.7–120 kg/s

assumed plasmoid production rate of one plasmoid per day, *Bagenal* [2007] calculated a mass loss rate of ~30 kg/s. Similarly, *Kronberg et al.* [2008b] used plasmoid sizes as measured by the Galileo energetic particle detector and other assumptions to calculate the plasmoid volume, 9 R_J long by 2 R_J high by 200 R_J wide, and then calculated the mass of each plasmoid as ~8×10^5 kg, assuming a number density of 0.025 particles/cm^3 and particle mass 16 m_p. (Note that the 9 R_J length reported by *Kronberg et al.* [2008a] is larger than the 2.6 R_J we estimated in section 4.2 because they defined the plasmoid interval as the time during which B_θ is enhanced, while we have defined the plasmoid interval as the time between the local maximum and local minimum in B_θ.)

Here we follow the works of *Bagenal* [2007] and *Kronberg et al.* [2008b] but with updated parameters based on the observed plasmoid properties from this study. Table 2 lists the required parameters and the corresponding values assumed in the previous studies. With only single-spacecraft measurements available, many of these parameters are subject to a large degree of uncertainty and we therefore include in our calculation the full range of values that can be supported by the observations. We assume a plasmoid azimuthal width of 45–70 R_J, as outlined in section 4.5. The observed plasmoid length was 2.6 R_J but this is likely to be an underestimate by as much as a factor of 5, as discussed in section 4.2, and we therefore take 2.6–20 R_J as an estimated range for the plasmoid length. The plasmoid height is relatively unconstrained, but we note that plasmoids at the Earth have a height of roughly twice the plasma sheet thickness [*Slavin et al.*, 1993], which is ~4–6 R_J [*Khurana and Schwarzl*, 2005] in Jupiter's postmidnight magnetosphere. We therefore assume a minimum plasmoid thickness of 2 R_J, following *Kronberg et al.* [2008b], and a maximum thickness of 12 R_J based on the maximum plasma sheet thickness.

We follow *Bagenal* [2007] in assuming a density of 0.01 particles/cm^3 (particle mass 20 m_p), which is consistent with the plasmoid density measurements reported by *Kasahara et al.* [2013]. We assume a plasmoid production rate of two to five plasmoids per day. In section 4.3 we discussed that the observations support a plasmoid production rate that may be as high as one plasmoid per day. Additionally, plasmoids are observed only when the spacecraft (at or near the Jovigraphic equator) is in or near the current sheet, which only occurs briefly (for about an hour) as the current sheet passes over the spacecraft every ~5 h due to Jupiter's 10° dipole tilt. Galileo's near-equatorial orbit in the postmidnight local time sector means that the spacecraft is within 4 R_J of the modeled current sheet center only ~30% of the time [*Khurana and Schwarzl*, 2005], suggesting that the observations may underestimate the plasmoid production rate by as much as a factor of 3–5. We therefore estimate the plasmoid production rate could therefore reasonably be two to five plasmoids per day.

From the above assumptions, we calculate a typical plasmoid mass of ~$28–2120 \times 10^3$ kg and a mass loss rate ranging from ~0.7 to ~120 kg/s. The typical amount of flux closed in the PPPS ranges from 3.7 to 13.7 GWb per plasmoid, depending on whether one uses the average value or the superposed epoch and on how one defines the PPPS interval. Assuming a plasmoid production rate of two to five plasmoids per day as in the mass loss calculation, the flux closure rate is then ~7–70 GWb per day.

How do the calculated mass output and flux closure rates compare to the estimated input values? The calculated mass loss rate, which is at most ~120 kg/s assuming the most generous plasmoid size and occurrence rates that can be supported by the observations, is at least a factor of 4–8 lower than the 500–1000 kg/s input rate from Io. Assuming midrange values for the plasmoid dimensions (10 R_J length, 60 R_J width, and 8 R_J height) and recurrence rate (three plasmoids per day) yields a mass loss rate of just ~30 kg/s, more than an order of magnitude smaller than the estimated input from Io. One possible explanation for the discrepancy is that errors in our assumptions for the plasmoid height, azimuthal width, or frequency, all of which are relatively unconstrained by the available single-spacecraft measurements, have caused us to underestimate the

plasmoid mass loss rate. However, attempting the same calculation using parameters for Earth's magnetosphere produces slightly better agreement between the plasmoid mass loss rate and the mass input rate from the solar wind, even considering only rough early estimates from single-spacecraft data that are subject to the same level of uncertainty in their interpretation as the Galileo data at Jupiter. Using ISEE 3 observations, *Slavin et al*. [1993] found the typical plasmoid mass is 280 kg and that more than one plasmoid may be produced per substorm (or equivalent reconnection episode) so that the plasmoid occurrence rate could be as high as one plasmoid per hour. This leads to a mass loss rate of ~0.078 kg/s. The solar wind transfers 10^{26}–10^{27} particles per second into the Earth's magnetosphere [*Pilipp and Morfill*, 1978; *Cowley*, 1980], which, assuming 1 amu per particle, results in a mass input rate of 0.17–1.7 kg/s. That the estimated mass input and output rates agree to within a factor of ~2 for the Earth but not for Jupiter (even in the most extreme case) suggests that errors in the plasmoid parameters alone are unlikely to explain why our calculated mass loss rate is so much lower than the input rate from Io.

Another explanation is that mass loss mechanisms other than plasmoid release dominate the magnetospheric mass transport at Jupiter, as suggested by *Bagenal* [2007]. These other proposed loss mechanisms include interchange motion [*Southwood and Kivelson*, 1987, 1989] across centrifugally unstable, highly stretched field lines in the dusk local time sector [*Kivelson and Southwood*, 2005], a planetary wind, and a ubiquitous but small-scale reconnection and plasmoid release ("drizzle") occurring across the tail [e.g., *Delamere and Bagenal*, 2010]. A full discussion of these proposed mechanisms is beyond the scope of this study, though we note that no observations of these specific processes have been reported, nor have there been any concrete estimates of what the resulting mass loss rate would be, and further work is called for. Finally, it is also possible that a significant amount of mass is lost through plasmoid release in the far dusk magnetotail, beyond the available spacecraft measurements, causing us to underestimate the plasmoid mass loss rate.

The calculated rate of open flux closure by plasmoids via the PPPS, ~7–70 GWb/d, shows relatively good agreement with the average rate of flux removal on the dayside through reconnection, which is an estimated ~18 GWb/d according to *Nichols et al*. [2006]. They used a formula that had been successfully applied at the Earth and later adapted to Saturn [*Jackman et al*., 2004], to calculate the dayside reconnection voltage at Jupiter, and estimated that 500 GWb of flux is opened via dayside reconnection during a solar rotation (27 days). This formula is highly sensitive to assumptions about the length of the region over which dayside reconnection can occur. Since the observed plasmoid flux closure rate matches the dayside flux opening rate, we can therefore conclude that tail reconnection and plasmoid release is an important method of flux transport at Jupiter. This is in contrast with the proposal from *McComas and Bagenal* [2007], who had suggested that return flow from tail reconnection at Jupiter would be difficult due to the large scale sizes in Jupiter's magnetosphere and opposition from outward plasma flow. They instead proposed that magnetic flux that is opened via dayside reconnection with the solar wind could be closed by reconnection at high latitudes on the magnetopause, near the polar cusps, rendering tail reconnection unnecessary. However, we find that the observed flux closure rates from the tail plasmoids is sufficient to balance the estimated rate at which flux is opened via reconnection on the dayside magnetopause and note also that *Cowley et al*. [2008] suggested that the proposed near-simultaneous reconnection at both the north and south cusps would be unlikely. We can compare the amount of flux opened or closed per day by reconnection to the ~720 GWb of open flux in the polar cap and tail lobes [*Vogt et al*., 2011] and find that it is only ~1–10%. Finally, we note that our average flux closure rate corresponds to a ~100–300 kV average reconnection voltage, which is small compared to the ~2–4 MV rotational flux transport voltage in the outer magnetosphere [e.g., *Badman and Cowley*, 2007].

5.2. Implications of the Inferred Plasmoid Structure

In section 4.4 we found that most plasmoids lack a core field and that the MVA results, though inconclusive due to the magnetometer data's low time resolution, matched the expected flux rope signature for only one plasmoid (on 14 June 1997). These findings have implications for our understanding of how Jovian plasmoids are formed. For instance, in the case of terrestrial flux ropes, the magnitude and direction of the core field are correlated with the IMF [*Moldwin and Hughes*, 1992], which at Jupiter is typically largely azimuthal, or at ~80° with respect to the Sun-Jupiter line [e.g., *Jackman and Arridge*, 2011], so a core azimuthal field would be expected. The lack of a core field in the Jovian plasmoids may therefore suggest that the IMF does not penetrate far enough into Jupiter's magnetosphere to influence plasmoid structure, which would raise

questions about the ability of the solar wind to drive tail reconnection in the first place. Alternatively, the plasmoids may be crater flux ropes, which contain an axial field but lack a central core field because they form in a high β plasma, such as that found in Jupiter's plasma sheet [e.g., *Walker et al*., 1978; *McNutt*, 1983; *Kane et al*., 1995, 1999].

5.3. Local Time Distribution of Reconnection Signatures

From a survey of all the Jovian reconnection signatures observed in magnetometer data, *Vogt et al*. [2010] concluded that reconnection is equally likely on either side of midnight. While the events are not evenly distributed in local time, after normalizing for the availability of data in the premidnight and postmidnight local time sectors, one finds that the event frequency is roughly equal near dawn and dusk but reaches a minimum at midnight. However, recent analysis of particle data from *Kasahara et al*. [2013] has suggested that the nature of the dusk and dawn events may differ, as only the dawn sector events displayed large density changes, indicating lobe reconnection, and large radial flows. Given these recent findings, and the fact that 42 of the 43 plasmoid signatures identified in the present study were observed postmidnight, it is appropriate to revisit the analysis of reconnection event frequency as a function of local time.

In calculating the event occurrence rate, *Vogt et al*. [2010] divided the duration of events in 1 h local time bins by the duration of all data in each bin. While this analysis accounted for differences in the amount of data available in each local time sector, it neglected the local time variation of the spacecraft radial coverage or the amount of time spent in or near the current sheet. For instance, few measurements are available beyond 90 R_J at duskside local times (1800 to 2200 h), as seen in Figure 6. Additionally, most reconnection events are observed when the spacecraft is in or near the current sheet, which is thickest near dusk and thinnest in the postmidnight to dawn local time sector [*Kivelson and Khurana*, 2002; *Waldrop et al*., 2005]. In the middle magnetosphere, the current sheet is located near the magnetic equator [*Khurana*, 1992], which is tilted ~10° with respect to the Jovigraphic equator. This means that a spacecraft located near the Jovigraphic equator, like Galileo, would at postmidnight local times spend most of its time in the magnetotail lobes, passing through the current sheet briefly every ~5 h (twice every Jovian rotation). By comparison, in the dusk local time sector, a spacecraft similarly located near the Jovigraphic equator may exit the current sheet only rarely, if at all, and therefore has a more favorable chance of observing reconnection signatures, which should be taken into consideration when calculating the event occurrence rate as a function of local time.

In order to obtain a rough but quantitative estimate of the fraction of time spent in or near the current sheet as a function of local time, we can compute the ratio of $|B_R|$ to $|B_\theta|$ and examine how often it is below a threshold value. In the magnetotail lobes, the magnetic field is predominantly in the radial direction and $|B_R/B_\theta|$ is large ($\gtrsim 10$), whereas the field is predominantly in the north–south direction in the current sheet and $|B_R|$ decreases, so $|B_R/B_\theta|$ is small. The fraction of time in which $|B_R/B_\theta|$ is below a threshold value can therefore provide a proxy for the fraction of time in which the spacecraft is located in or near the current sheet. Figure 12a shows the fraction of time that $|B_R/B_\theta|$ is below a given value plotted versus local time. As in the event identification procedure used by *Vogt et al*. [2010], in making this plot we have restricted ourselves to data within 15° of the equatorial plane and with time resolution 60 s per vector or better. Furthermore, we included data only inside of 90 R_J, where the availability of data is relatively even across nightside local times. The figure shows that $|B_R/B_\theta|$ is small, indicating that the spacecraft is likely in or near the current sheet, very frequently at premidnight local times but only ~20% of the time postmidnight. This can be used to normalize the event occurrence rate as a function of local time.

The red dashed line in Figure 12b shows the event occurrence rate calculated by *Vogt et al*. [2010] using reconnection events and data from all radial distances. Without accounting for the local time dependence of the amount of time spent near the current sheet, the event occurrence rate is roughly equal on either side of midnight. The black solid line in Figure 12b shows the event occurrence rate that has been normalized by the fraction of time in which $|B_R/B_\theta|$ is below a threshold value (from Figure 12a), and including events and data only inside of 90 R_J. Here we used the criterion $|B_R/B_\theta| \leq 6$ to define the time spent in or near the current sheet and calculate a normalization factor, though any of the $|B_R/B_\theta|$ values from of Figure 12a would have produced similar results. Additionally, we defined the normalization factor so that the event occurrence rate in the 0230–0330 h local time bin is equal for both cases. The figure shows that, after accounting for the fact that the spacecraft spends more time near the current sheet premidnight than postmidnight, the normalized event frequency inside of 90 R_J is then much higher postmidnight than premidnight.

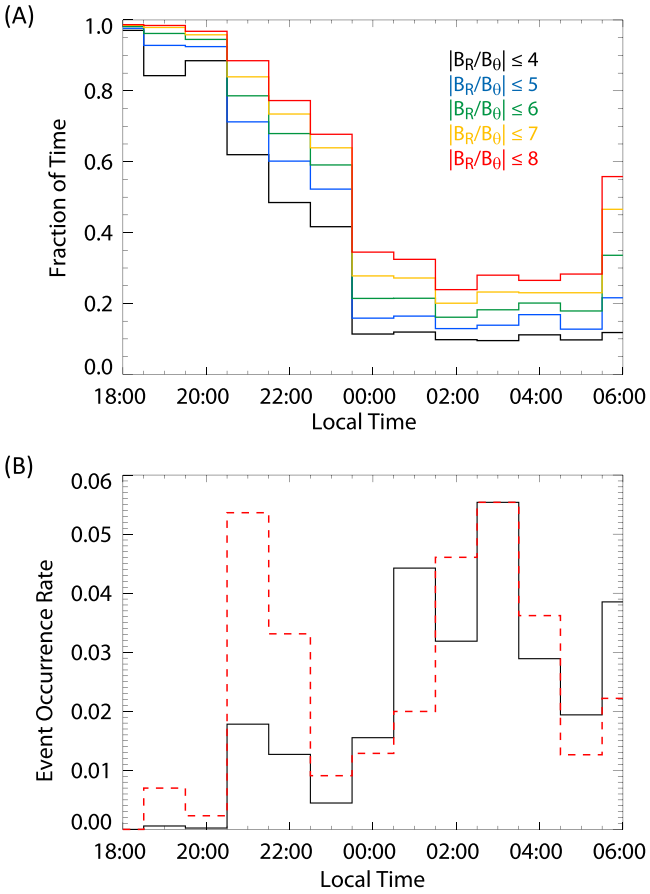

Figure 12. (a) Fraction of time that $|B_R/B_\theta|$ is below various threshold values inside of 90 R_J, plotted as a function of local time. This quantity is a proxy for the fraction of time that the spacecraft is located in or near the current sheet (see text). (b) The dashed red line shows the event occurrence rate as a function of local time [from *Vogt et al.*, 2010, Figure 10], which is roughly equal on either side of midnight. The black solid line shows the same event occurrence rate, but normalized (see text) to account for the fraction of time spent in or near the current sheet in each local time bin in Figure 12a and including only events and data from inside 90 R_J.

This new insight that the event frequency varies across local time sectors is directly relevant to the question of which factors are responsible for driving dynamics in Jupiter's magnetotail. For example, it has been proposed that Dungey cycle-driven reconnection may be restricted to the postmidnight local time sector because the strong outward flows associated with corotation and the Vasyliūnas cycle would oppose sunward return flow from a reconnection X-line [*Cowley et al.*, 2003]. The observation that reconnection signatures are more frequent in the dawn sector, where they also display larger density changes and radial flows [*Kasahara et al.*, 2013], compared to the dusk sector is therefore suggestive that the solar wind may be the primary driver behind tail reconnection at Jupiter. However, it should also be noted that dawn-dusk asymmetries have been observed in the rate of plasmoid occurrence at the Earth, where the Dungey cycle alone is responsible for driving tail reconnection [e.g., *Imber et al.*, 2011]. We cannot rule out the importance of internal driving. Reconnection signatures are most easily observed near the statistical X-line, which is located at ~90 R_J near dawn and farther out near midnight. It is therefore possible that the duskside reconnection signatures are observed less frequently and are less pronounced in the particle data simply because the duskside data were collected far from the reconnection site, and that the local time asymmetries discussed here result from strong local time dependence of the neutral line location coupled with limitations of radial coverage. Additionally, it is likely to be more difficult to detect plasmoid signatures on the duskside because of the large amplitude of field fluctuations in the thick plasma sheet. This effect would counteract the normalization due to time spent near the current sheet we have done here. Future observations including simultaneous upstream solar wind and magnetotail measurements, and improved coverage of the premidnight local time sector, are required to establish which of these explanations is valid.

6. Summary

In this study we have examined the statistical properties and interior structure of plasmoid signatures found in magnetometer data from Jupiter's magnetotail. We selected 43 tailward moving plasmoids from a larger list of 249 reconnection events, which had been identified in a previous study by an increase in $|B_\theta|$, indicating a field dipolarization, by at least a factor of 2 over background levels. The plasmoids all display a characteristic bipolar signature in which B_θ, initially southward, becomes enhanced over background levels, then reverses (turns northward). If the field remains northward for an extended interval following the central plasmoid signature, defined as the time between the maximum and minimum in $|B_\theta|$, this interval is called the postplasmoid plasma sheet (PPPS) and it can be used to estimate the amount of open flux closed.

We performed a superposed epoch analysis on the 43 plasmoids studied here and compiled statistics on their average properties, including location, recurrence time, and length scale. We have also placed an upper limit on the amount of flux closed in the PPPS by assuming that the PPPS signature is produced by the reconnection of open lobe field lines and not due to other effects such as an oblique spacecraft trajectory or deceleration as the plasmoids move down the tail. All but one of the 43 plasmoids from this study were located in the postmidnight local time sector, with most located between 01:30 and 03:00 LT, at an average radial distance of 94 R_J, near the location of a statistical separatrix. New analysis of the reconnection event frequency as a function of local time inside of 90 R_J also found that reconnection signatures are most likely in the postmidnight local time sector. The typical plasmoid recurrence time is a few days, though many plasmoids appeared in chains or pairs, separated by less than an hour. Additionally, most plasmoids were observed during three orbits during the Galileo mission, G2 in September to October 1996, G8 in May to June 1997, and C10 in October 1997, though it remains unclear whether the dynamic nature of these orbits resulted from external conditions or whether the orbits took the spacecraft through a particularly dynamic region of the magnetosphere. The superposed epoch analysis showed an extended PPPS interval, and we calculated that a typical plasmoid event can close a maximum of 3.7 to 13.7 GWb of open flux.

Visual inspection showed that most Jovian plasmoids lack a core field, suggesting the plasmoids are magnetic loops or possibly crater flux ropes. We used minimum variance analysis to examine the structure of the four plasmoids that did have core fields; though most of the hodograms were inconclusive due to the plasmoids' short duration and low time resolution of the magnetic field data. However, one plasmoid (of 43) appeared to have a flux rope structure. At the Earth, the presence or absence of a core field is correlated with the IMF direction, being most likely at times when the IMF has a strong azimuthal or east–west component. A core azimuthal field may be expected in Jovian plasmoids because the IMF is typically azimuthal near Jupiter. The absence of a core field therefore could suggest that the IMF does not penetrate far enough into Jupiter's magnetosphere to influence plasmoid structure.

In order to understand the role of plasmoids in the overall mass and flux transport in Jupiter's magnetosphere, we calculated the mass loss and flux closure rates using the average plasmoid properties. These calculations required estimates for some quantities, such as the plasmoid azimuthal extent and frequency, which are relatively underconstrained by the observations. Therefore in our calculation, we included the full range of values for the plasmoid dimensions and recurrence rates that are consistent with the available observations. We estimated that the typical plasmoid mass loss rate ranges from ~0.7 to ~120 kg/s, much lower than the mass input rate from Io (500–1000 kg/s). While some of the difference between the estimated input and output rates could be accounted for by incorrect assumptions about the plasmoid size, density, or recurrence period, it appears likely that the observed plasmoids play a limited role in the magnetospheric mass transport process at Jupiter. Further work is called for to investigate other potential mass loss mechanisms. In contrast to the mass loss rate, the estimated flux closure rate, ~7–70 GWb/d, closely matches the estimated rate of average flux opening through dayside reconnection, 18 GWb/d. We therefore conclude that tail reconnection and plasmoids play an important role in flux transport at Jupiter.

Acknowledgments

This work was conceived during two meetings of the International Space Science Institute (ISSI) "Dynamics of Planetary Magnetotails" team number 195, of which M.F.V., C.M.J., and J.A.S. were members. M.F.V. gratefully acknowledges helpful discussions with several other team members, including Aikaterina Radioti for consultation regarding the auroral polar dawn spots and Fran Bagenal. M.F.V., E.J.B., and S.W.H.C. were supported by the UK Science & Technology Facilities Council (STFC) Consolidated grant ST/K001000/1. E.J.B. was also supported by the 2011 Philip Leverhulme Prize. C.M.J. was supported by a Leverhulme Trust Early Career Fellowship and a Royal Astronomical Society Fellowship.

Masaki Fujimoto thanks Raymond Walker and an anonymous reviewer for their assistance in evaluating this paper.

References

Angelopoulos, V., C. F. Kennel, F. V. Coroniti, R. Pellat, M. G. Kivelson, R. J. Walker, C. T. Russell, W. Baumjohann, W. C. Feldman, and J. T. Gosling (1994), Statistical characteristics of bursty bulk flow events, *J. Geophys. Res.*, *99*, 21,257–21,280, doi:10.1029/94JA01263.

Angelopoulos, V., et al. (2008), Tail reconnection triggering substorm onset, *Science*, *321*, 931–935, doi:10.1126/science.1160495.

Angelopoulos, V., et al. (1996), Multipoint analysis of a bursty bulk flow event on April 11, 1985, *J. Geophys. Res.*, *101*, 4967–4989, doi:10.1029/95JA02722.

Badman, S. V., and S. W. H. Cowley (2007), Significance of Dungey-cycle flows in Jupiter's and Saturn's magnetospheres, and their identification on closed equatorial field lines, *Ann. Geophys.*, *25*, 941–951.
Bagenal, F. (2007), The magnetosphere of Jupiter: Coupling the equator to the poles, *J. Atmos. Sol. Terr. Phys.*, *69*, 387–402, doi:10.1016/j.jastp.2006.08.012.
Bagenal, F., and P. A. Delamere (2011), Flow of mass and energy in the magnetospheres of Jupiter and Saturn, *J. Geophys. Res.*, *116*, A05209, doi:10.1029/2010JA016294.
Borg, A. L., M. G. G. T. Taylor, and J. P. Eastwood (2012), Observations of magnetic flux ropes during magnetic reconnection in the Earth's magnetotail, *Ann. Geophys.*, *30*, 761–773, doi:10.5194/angeo-30-761-2012.
Cowley, S. W. H. (1980), Plasma populations in a simple open model magnetosphere, *Space Sci. Rev.*, *26*, 217–275.
Cowley, S. W. H., E. J. Bunce, T. S. Stallard, and S. Miller (2003), Jupiter's polar ionospheric flows: Theoretical interpretation, *Geophys. Res. Lett.*, *30*(5), 1220, doi:10.1029/2002GL016030.
Cowley, S. W. H., S. V. Badman, S. M. Imber, and S. E. Milan (2008), Comment on "Jupiter: A fundamentally different magnetospheric interaction with the solar wind" by D. J. McComas and F. Bagenal, *Geophys. Res. Lett.*, *35*, L10101, doi:10.1029/2007GL032645.
Delamere, P. A., and F. Bagenal (2010), Solar wind interaction with Jupiter's magnetosphere, *J. Geophys. Res.*, *115*, A10201, doi:10.1029/2010JA015347.
Farrugia, C. J., R. P. Rijnbeek, M. A. Saunders, D. J. Southwood, D. J. Rodgers, M. F. Smith, C. P. Chaloner, D. S. Hall, P. J. Christiansen, and L. J. C. Woolliscroft (1988), A multi-instrument study of flux transfer event structure, *J. Geophys. Res.*, *93*, 14,465–14,477.
Fukazawa, K., T. Ogino, and R. J. Walker (2005), Dynamics of the Jovian magnetosphere for northward interplanetary magnetic field (IMF), *Geophys. Res. Lett.*, *32*, L03202, doi:10.1029/2004GL021392.
Fukazawa, K., T. Ogino, and R. J. Walker (2006), Configuration and dynamics of the Jovian magnetosphere, *J. Geophys. Res.*, *111*, A10207, doi:10.1029/2006JA011874.
Fukazawa, K., T. Ogino, and R. J. Walker (2010), A simulation study of dynamics in the distant Jovian magnetotail, *J. Geophys. Res.*, *115*, A09219, doi:10.1029/2009JA015228.
Ge, Y. S., L. K. Jian, and C. T. Russell (2007), Growth phase of Jovian substorms, *Geophys. Res. Lett.*, *34*, L23106, doi:10.1029/2007GL031987.
Grodent, D., J.-C. Gérard, J. T. Clarke, G. R. Gladstone, and J. H. Waite (2004), A possible auroral signature of a magnetotail reconnection process on Jupiter, *J. Geophys. Res.*, *109*, A05201, doi:10.1029/2003JA010341.
Hill, T. W., A. J. Dessler, and C. K. Goertz (1983), Magnetospheric models, in *Physics of the Jovian Magnetosphere*, edited by A. J. Dessler, pp. 395, Cambridge Univ. Press, New York.
Hones, E. W., Jr. (1976), The magnetotail: Its generation and dissipation, in *Physics of Solar Planetary Environments*, edited by D. J. Williams, pp. 559–571, AGU, Washington, D. C.
Hones, E. W., Jr. (1977), Substorm processes in the magnetotail: Comments on "On hot tenuous plasma, fireballs, and boundary layers in the Earth's magnetotail" by L.A. Frank, K. L. Ackerson, and R. P. Lepping, *J. Geophys. Res.*, *82*, 5633–5640, doi:10.1029/JA082i035p05633.
Hughes, W. J., and D. G. Sibeck (1987), On the 3-dimensional structure of plasmoids, *Geophys. Res. Lett.*, *14*, 636–639, doi:10.1029/GL014i006p00636.
Ieda, A., S. Machida, T. Mukai, Y. Saito, T. Yamamoto, A. Nishida, T. Terasawa, and S. Kokubun (1998), Statistical analysis of the plasmoid evolution with Geotail observations, *J. Geophys. Res.*, *103*, 4453–4465.
Imber, S. M., J. A. Slavin, H. U. Auster, and V. Angelopoulos (2011), A THEMIS survey of flux ropes and traveling compression regions: Location of the near-Earth reconnection site during solar minimum, *J. Geophys. Res.*, *116*, A02201, doi:10.1029/2010JA016026.
Jackman, C. M., and C. S. Arridge (2011), Solar cycle effects on the dynamics of Jupiter's and Saturn's magnetospheres, *Solar Phys.*, *274*, 481–502.
Jackman, C. M., N. Achilleos, E. J. Bunce, S. W. H. Cowley, M. K. Dougherty, G. H. Jones, S. E. Milan, and E. J. Smith (2004), Interplanetary magnetic field at ~ 9 AU during the declining phase of the solar cycle and its implications for Saturn's magnetospheric dynamics, *J. Geophys. Res.*, *109*, A11203, doi:10.1029/2004JA010614.
Jackman, C. M., C. T. Russell, D. J. Southwood, C. S. Arridge, N. Achilleos, and M. K. Dougherty (2007), Strong rapid dipolarizations in Saturn's magnetotail: In situ evidence of reconnection, *Geophys. Res. Lett.*, *34*, L11203, doi:10.1029/2007GL029764.
Jackman, C. M., J. A. Slavin, and S. W. H. Cowley (2011), Cassini observations of plasmoid structure and dynamics: Implications for the role of magnetic reconnection in magnetospheric circulation at Saturn, *J. Geophys. Res.*, *116*, A10212, doi:10.1029/2011JA016682.
Jia, X., K. C. Hansen, T. I. Gombosi, M. G. Kivelson, G. Tóth, D. L. DeZeeuw, and A. J. Ridley (2012), Magnetospheric configuration and dynamics of Saturn's magnetosphere: A global MHD simulation, *J. Geophys. Res.*, *117*, A05225, doi:10.1029/2012JA017575.
Joy, S. P., M. G. Kivelson, R. J. Walker, K. K. Khurana, C. T. Russell, and T. Ogino (2002), Probabilistic models of the Jovian magnetopause and bow shock locations, *J. Geophys. Res.*, *107*, 1309, doi: 10.1029/2001JA009146.
Kane, M., B. H. Mauk, E. P. Keath, and S. M. Krimigis (1995), Hot ions in Jupiter's magnetodisc: A model for Voyager 2 low-energy charged particle measurements, *J. Geophys. Res.*, *100*, 19,473–19,486.
Kane, M., D. J. Williams, B. H. Mauk, R. W. McEntire, and E. C. Roelof (1999), Galileo Energetic Particles Detector measurements of hot ions in the neutral sheet region of Jupiter's magnetodisk, *Geophys. Res. Lett.*, *26*, 5–8.
Kasahara, S., E. A. Kronberg, T. Kimura, C. Tao, S. V. Badman, A. Masters, A. Retinò, N. Krupp, and M. Fujimoto (2013), Asymmetric distribution of reconnection jet fronts in the Jovian nightside magnetosphere, *J. Geophys. Res. Space Physics*, *118*, 375–384, doi:10.1029/2012JA018130.
Khurana, K. K. (1992), A generalized hinged-magnetodisc model of Jupiter's nightside current sheet, *J. Geophys. Res.*, *97*, 6269–6276.
Khurana, K. K., and H. K. Schwarzl (2005), Global structure of Jupiter's magnetospheric current sheet, *J. Geophys. Res.*, *110*, A07227, doi:10.1029/2004JA010757.
Kivelson, M. G., and K. K. Khurana (1995), Models of flux ropes embedded in a Harris neutral sheet: Force-free solutions in low and high beta plasmas, *J. Geophys. Res.*, *100*, 23,637–23,645.
Kivelson, M. G., and K. K. Khurana (2002), Properties of the magnetic field in the Jovian magnetotail, *J. Geophys. Res.*, *107*(A8), 1196, doi:10.1029/2001JA000249.
Kivelson, M. G., and D. J. Southwood (2005), Dynamical consequences of two modes of centrifugal instability in Jupiter's outer magnetosphere, *J. Geophys. Res.*, *110*, A12209, doi:10.1029/2005JA011176.
Kronberg, E. A., J. Woch, N. Krupp, A. Lagg, K. K. Khurana, and K.-H. Glassmeier (2005), Mass release at Jupiter: Substorm-like processes in the Jovian magnetotail, *J. Geophys. Res.*, *110*, A03211, doi:10.1029/2004JA010777.
Kronberg, E. A., K.-H. Glassmeier, J. Woch, N. Krupp, A. Lagg, and M. K. Dougherty (2007), A possible intrinsic mechanism for the quasi-periodic dynamics of the Jovian magnetosphere, *J. Geophys. Res.*, *112*, A05203, doi:10.1029/2006JA011994.

Kronberg, E. A., J. Woch, N. Krupp, and A. Lagg (2008a), Mass release process in the Jovian magnetosphere: Statistics on particle burst parameters, *J. Geophys. Res.*, *113*, A10202, doi:10.1029/2008JA013332.
Kronberg, E. A., J. Woch, N. Krupp, A. Lagg, P. W. Daly, and A. Korth (2008b), Comparison of periodic substorms at Jupiter and Earth, *J. Geophys. Res.*, *113*, A04212, doi:10.1029/2007JA012880.
Kronberg, E. A., J. Woch, N. Krupp, and A. Lagg (2009), A summary of observational records on periodicities above the rotational period in the Jovian magnetosphere, *Ann. Geophys.*, *27*, 2565–2573.
Krupp, N., J. Woch, A. Lagg, B. Wilken, S. Livi, and D. J. Williams (1998), Energetic particle bursts in the predawn Jovian magnetotail, *Geophys. Res. Lett.*, *25*, 1249–1252.
McComas, D. J., and F. Bagenal (2007), Jupiter: A fundamentally different magnetospheric interaction with the solar wind, *Geophys. Res. Lett.*, *34*, L20106, doi:10.1029/2007GL031078.
McNutt, R. L., Jr. (1983), Force balance in the magnetospheres of Jupiter and Saturn, *Adv. Space Res.*, *3*, 55–58.
Moldwin, M. B., and W. J. Hughes (1992), On the formation and evolution of plasmoids: A survey of ISEE 3 Geotail data, *J. Geophys. Res.*, *97*, 19,259–19,282, doi:10.1029/92JA01598.
Nichols, J. D., S. W. H. Cowley, and D. J. McComas (2006), Magnetopause reconnection rate estimates for Jupiter's magnetosphere based on interplanetary measurements at ~5 AU, *Ann. Geophys.*, *24*, 393–406.
Nishida, A. (1983), Reconnection in the Jovian magnetosphere, *Geophys. Res. Lett.*, *10*, 451–454.
Pilipp, W. G., and G. Morfill (1978), The formation of the plasma sheet resulting from plasma mantle dynamics, *J. Geophys. Res.*, *83*, 5670–5678.
Radioti, A., D. Grodent, J.-C. Gérard, B. Bonfond, and J. T. Clarke (2008), Auroral polar dawn spots: Signatures of internally driven reconnection processes at Jupiter's magnetotail, *Geophys. Res. Lett.*, *35*, L03104, doi:10.1029/2007GL032460.
Radioti, A., D. Grodent, J.-C. Gérard, and B. Bonfond (2010), Auroral signatures of flow bursts released during magnetotail reconnection at Jupiter, *J. Geophys. Res.*, *115*, A07214, doi:10.1029/2009JA014844.
Radioti, A., D. Grodent, J.-C. Gérard, M. F. Vogt, M. Lystrup, and B. Bonfond (2011), Nightside reconnection at Jupiter: Auroral and magnetic field observations from July 26, 1998, *J. Geophys. Res.*, *116*, A03221, doi:10.1029/2010JA016200.
Richardson, I. G., S. W. H. Cowley, E. W. Hones Jr., and S. J. Bame (1987), Plasmoid-associated energetic ion bursts in the deep geomagnetic tail: Properties of plasmoids and the postplasmoid plasma sheet, *J. Geophys. Res.*, *92*, 9997–10,013.
Russell, C. T., and R. C. Elphic (1978), Initial ISEE magnetometer results: Magnetopause observations, *Space Sci. Rev.*, *22*, 681–715.
Russell, C. T., K. K. Khurana, D. E. Huddleston, and M. G. Kivelson (1998), Localized reconnection in the near Jovian magnetotail, *Science*, *280*, 1061–1064.
Sharma, A. S., et al. (2008), Transient and localized processes in the magnetotail: A review, *Ann. Geophys.*, *26*, 955–1006.
Slavin, J. A., M. F. Smith, E. L. Mazur, D. N. Baker, E. W. Hones Jr., T. Iyemori, and E. W. Greenstadt (1993), ISEE 3 observations of traveling compression regions in the Earth's magnetotail, *J. Geophys. Res.*, *98*, 15,425–15,446.
Slavin, J. A., et al. (1997), WIND, GEOTAIL, and GOES 9 observations of magnetic field dipolarization and bursty bulk flows in the near-tail, *Geophys. Res. Lett.*, *24*, 971–974.
Slavin, J. A., R. P. Lepping, J. Gjerloev, D. H. Fairfield, M. Hesse, C. J. Owen, M. B. Moldwin, T. Nagai, A. Ieda, and T. Mukai (2003a), Geotail observations of magnetic flux ropes in the plasma sheet, *J. Geophys. Res.*, *108*(A1), 1015, doi:10.1029/2002JA009557.
Slavin, J. A., et al. (2003b), Cluster electric current density measurements within a magnetic flux rope in the plasma sheet, *Geophys. Res. Lett.*, *30*(7), 1362, doi:10.1029/2002GL016411.
Slavin, J. A., et al. (2009), MESSENGER observations of magnetic reconnection in Mercury's magnetosphere, *Science*, *324*, 606–610, doi:10.1126/science.1172011.
Slavin, J. A., et al. (2012), MESSENGER and Mariner 10 flyby observations of magnetotail structure and dynamics at Mercury, *J. Geophys. Res.*, *117*, A01215, doi:10.1029/2011JA016900.
Sonnerup, B. U. Ö., and L. J. Cahill Jr. (1967), Magnetopause structure and attitude from Explorer 12 observations, *J. Geophys. Res.*, *72*, 171–183.
Southwood, D. J., and M. G. Kivelson (1987), Magnetospheric interchange instability, *J. Geophys. Res.*, *92*, 109–116, doi:10.1029/JA092iA01p00109.
Southwood, D. J., and M. G. Kivelson (1989), Magnetospheric interchange motions, *J. Geophys. Res.*, *94*, 299–308, doi:10.1029/JA094iA01p00299.
Thomas, N., F. Bagenal, T. W. Hill, and J. K. Wilson (2004), The Io neutral cloud and plasma torus, in *Jupiter: The Planet, Satellites, and Magnetosphere*, edited by F. Bagenal et al., pp. 561–591, Cambridge Univ. Press, New York.
Vasyliūnas, V. M. (1983), Plasma distribution and flow, in *Physics of the Jovian Magnetosphere*, edited by A. J. Dessler, pp. 395, Cambridge Univ. Press, New York.
Vogt, M. F., M. G. Kivelson, K. K. Khurana, S. P. Joy, and R. J. Walker (2010), Reconnection and flows in the Jovian magnetotail as inferred from magnetometer observations, *J. Geophys. Res.*, *115*, A06219, doi:10.1029/2009JA015098.
Vogt, M. F., M. G. Kivelson, K. K. Khurana, R. J. Walker, B. Bonfond, D. Grodent, and A. Radioti (2011), Improved mapping of Jupiter's auroral features to magnetospheric sources, *J. Geophys. Res.*, *116*, A03220, doi:10.1029/2010JA016148.
Waldrop, L. S., T. A. Fritz, M. G. Kivelson, K. Khurana, N. Krupp, and A. Lagg (2005), Jovian plasma sheet morphology: Particle and field observations by the Galileo spacecraft, *Planet. Space Sci.*, *53*, 681–692.
Walker, R. J., M. G. Kivelson, and A. W. Schardt (1978), High β plasma in the dynamic Jovian current sheet, *Geophys. Res. Lett.*, *5*, 799–802.
Woch, J., N. Krupp, A. Lagg, B. Wilken, S. Livi, and D. J. Williams (1998), Quasiperiodic modulations of the Jovian magnetotail, *Geophys. Res. Lett.*, *25*, 1253–1256, doi:10.1029/98GL00861.
Woch, J., N. Krupp, and A. Lagg (2002), Particle bursts in the Jovian magnetosphere: Evidence for a near-Jupiter neutral line, *Geophys. Res. Lett.*, *29*(7), 1138, doi:10.1029/2001GL014080.
Zhang, H., et al. (2010), Evidence that crater flux transfer events are initial stages of typical flux transfer events, *J. Geophys. Res.*, *115*, A08229, doi:10.1029/2009JA015013.
Zieger, B., K. C. Hansen, T. I. Gombosi, and D. L. De Zeeuw (2010), Periodic plasma escape from the mass-loaded Kronian magnetosphere, *J. Geophys. Res.*, *115*, A08208, doi:10.1029/2009JA014951.